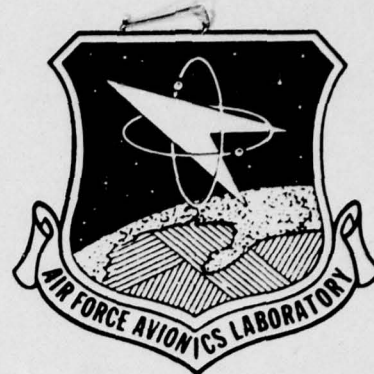| OF |
ADA
042985

END
DATE
FILMED

9-77

DDC

AFAL-TR-76-230
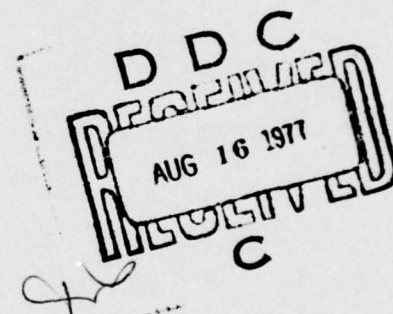
MAGNETO-OPTIC DEVELOPMENT FOR LASER BEAM STEERING

SPERRY UNIVAC
ST. PAUL, MINNESOTA 55165

MAY 1977

TECHNICAL REPORT AFAL-TR-76-230
FINAL REPORT FOR PERIOD MARCH 1975 - MAY 1976

AIR FORCE AVIONICS LABORATORY
AIR FORCE WRIGHT AERONAUTICAL LABORATORIES
AIR FORCE SYSTEMS COMMAND
WRIGHT-PATTERSON AIR FORCE BASE, OHIO 45433
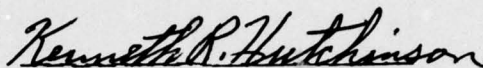
NOTICE

This technical report has been reviewed and is approved for publication.

LESLIE J. LAWRENCE
PROJECT ENGINEER
ELECTRO-OPTICS TECHNIQUES AND
  APPLICATIONS GROUP

KENNETH R. HUTCHINSON, CHIEF
ELECTRO-OPTICS TECHNIQUES AND
  APPLICATIONS GROUP
ELECTRO-OPTICS TECHNOLOGY BRANCH

WILLIAM C. SCHOONOVER, CHIEF
ELECTRO-OPTICS TECHNOLOGY BRANCH
ELECTRONIC TECHNOLOGY DIVISION

AIR FORCE - 28 JUN 77 - 100

REPORT DOCUMENTATION PAGE	READ INSTRUCTIONS BEFORE COMPLETING FORM

1. REPORT NUMBER	2. GOVT ACCESSION NO.	3. RECIPIENT'S CATALOG NUMBER
AFAL-TR-76-230		

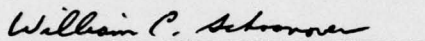| 4. TITLE (and Subtitle)	5. TYPE OF REPORT & PERIOD COVERED
MAGNETO-OPTIC DEVELOPMENT FOR LASER BEAM STEERING.	Technical rept. March 75— May 76
	6. PERFORMING ORG. REPORT NUMBER

7. AUTHOR(s)	8. CONTRACT OR GRANT NUMBER(s)
T. R. Johansen, F. G. Hewitt, J. Krawczak, and E. J. Torok	F33615-75-C-1099

9. PERFORMING ORGANIZATION NAME AND ADDRESS	10. PROGRAM ELEMENT, PROJECT, TASK AREA & WORK UNIT NUMBERS
Sperry Univac St. Paul, Minnesota 55165	2001-02-29

11. CONTROLLING OFFICE NAME AND ADDRESS	12. REPORT DATE
Air Force Avionics Laboratory AFAL/DHO Wright-Patterson AFB, Ohio 45433	May 1977
	13. NUMBER OF PAGES
	62

14. MONITORING AGENCY NAME & ADDRESS(if different from Controlling Office)	15. SECURITY CLASS. (of this report)
62 p.	Unclassified
	15a. DECLASSIFICATION/DOWNGRADING SCHEDULE

16. DISTRIBUTION STATEMENT (of this Report)

Approved for public release: distribution unlimited.

17. DISTRIBUTION STATEMENT (of the abstract entered in Block 20, if different from Report)

DDC AUG 16 1977

18. SUPPLEMENTARY NOTES

19. KEY WORDS (Continue on reverse side if necessary and identify by block number)

Magneto-optic laser beam steering
Bismuth Substituted rare earth iron garnet

20. ABSTRACT (Continue on reverse side if necessary and identify by block number)

Wide angle laser beam steering is required for numerous applications which require the collimation and brightness of laser beams. To this end, an effort to develop magneto-optic laser beam steering based on magnetic stripe domain diffraction has been conducted.

over

DD FORM 1 JAN 73 **1473** EDITION OF 1 NOV 65 IS OBSOLETE

It was discovered that strain-free bismuth-substituted rare earth iron garnet crystals can be grown by liquid phase epitaxy on gadolinium gallium garnet provided that sodium oxide or lead oxide is added to the bismuth oxide solvent melt. The function of the sodium or lead oxide is to increase the amount of elastic compressive strain a growing crystal film can support and yet at the same time maintain perfect lattice registry with the substrate crystal. In this way the strain which develops during cooling to room temperature after growth is cancelled. Thus, the epitaxial crystal does not fracture despite the large thermal expansion coefficient mismatch which exists between bismuth rare earth iron garnet crystals and the gadolinium garnet substrate material. Of course, the growth of strain free crystals is aided by utilizing as low a growth temperature as practical.

The characterization of the crystals shows that they are well suited for laser beam steering especially at 1.06 μm wavelength. The desired large Faraday rotation, 25,000°/cm at 6328 Å, and 3000°/cm at 1.06 μm, was obtained. Furthermore, some of the crystals are relatively transparent at 1.06 μm wavelength. Absorption coefficients of 10-100db/cm are typical of the best whereas coefficients more than 1000 db/cm were noted for some of the least transparent. The exact cause of the absorption is not known; the cause is probably electronic transitions between localized band gap states which are due to chemical impurities. The high rotation and high transparency indicate that with the existing crystals a 50% efficient beam steering device for 1.06 μm is possible.

The magnetic properties of the bismuth garnet crystals are ideal for stripe domain formation. The high magnetization, 1000 to 1800 Gauss, and the low normal anistropy, $\approx$ 50-100 Oe, are well suited to low drive power steering devices.

The scatter structure of the first order diffracted beam has been associated with a stripe grating perturbation in the form of a vertex domain structure. The vertices divide the grating into separate, uniform regions and move in response to changes in drive field. Vertex domains are not necessary for grating periodicity changes; however, whenever they occur, they must be kept out of the beam aperture. Vertex domain grating perturbations can cause a 10 mr beam divergence.

FOREWORD

This report was prepared by Sperry Univac, Applied Physics Laboratory, Univac Park, St. Paul, Minnesota, under Project Number 2001, Contract Number F33615-75-C-1099. The work was administered by the Air Force Avionics Laboratory, with Mr. Leslie J. Lawrence, AFAL/DHO, as Project Administrator.

This summary report covers research conducted from 1 March 1975 through 1 May 1976 in the Applied Physics Laboratory, A. D. Kaske, Manager. Members of the laboratory personnel who participated are: T. R. Johansen, E. J. Torok, J. Krawczak, F. Hewitt, G. Nelson, D. Fleming, and E. W. Simon. The report is submitted by the authors in July 1976.

TABLE OF CONTENTS

v

LIST OF ILLUSTRATIONS

SECTION I
INTRODUCTION

Following the discovery and development of the laser, applications which utilize the brighness and collimation of laser beams have proliferated. Many of the applications require wide angle, high resolution laser beam steering. One such application is laser recording; other applications are scanning, communications, target designation, optical processing, and optical computer memories.

The objective of this program is to explore the operating characteristics of the magneto-optic laser beam steering. The method of beam steering has several unique features which would simplify the optical arrangements of proposed systems.

This effort is to explore magneto-optic laser beam steering: to measure the optical, the magnetic, and the physical characteristics of magneto-optic materials to a degree which will allow design of useful devices. This effort does not include testing of new material formulations but only the preparation and examination of materials which have been shown in the past to possess the necessary characteristics to be of interest for optical beam steering at laser wavelengths.

Many laser applications have been proposed to take advantage of the high brightness and excellent collimation of laser optical sources. However, in order to provide improved systems based on the optical properties of laser radiation, accurate and predictable directional control of this radiation is needed. At high scan rates, such as those needed for image recording, electrically driven, non-moving beam steering methods are preferred.

Rotating prismatic mirrors are the common method for steering optical radiation. Such systems perform adequately at slow scan rates but encounter difficulties at the high scan rates needed for image recording. At 60,000 to 100,000 rpm, prisms show physical distortion due to centrifugal force and scan synchronization is difficult to maintain. Rotating optical elements are limited to beam steering in only one direction with no random access capability.

1

Magneto-optic laser beam steering by means of the Faraday effect or the magneto-optic Kerr effect in stripe domains has been shown to possess characteristics which tend to overcome or circumvent problems which limit other techniques. Laser beam steering in two orthogonal directions with a single device has been shown to be possible with low power consumption.[1,2,3]

A magneto-optic light deflector based on the stripe domain phenomena is inherently a wide angle, two dimensional, high resolution deflector. Diffraction of a light beam occurs as a result of a periodic variation in the wave amplitude or phase across a wave normal surface. Magnetic stripe domains can introduce a periodic 180° phase variation in a light beam. Consider an array of stripe domains in a magnetic platelet and a light beam propagating normal to the platelet, Figure 1. A stripe domain is a long, straight region of uniform width in which the magnetization vector is nearly constant. In an array of parallel stripe domains the magnetization in every domain has one component which is in the plane of the platelet and parallel to the stripe direction (see Figure 1, where the domains are parallel to the x-axis). This component has a constant magnitude everywhere in the arra causes the stripes to line up with the applied magnetic field. The other magneti ponent which is normal to the plane of the platelet introduces the perio riation in the light beam. This component points parallel to the z-axis in the odd numbered domains and the opposite way, antiparallel to the z-axis in the even-numbered domains (see Figure 1). Since the sense of the magneto-optic polarization rotation depends on whether the light propagates parallel or antiparallel to the magneti-zation, this arrangement produces a differential Faraday rotation between light passing through the even-numbered domains and the light passing through the odd-numbered domains. The differentially rotated light beam has an electric component which is orthogonal to the incident electric vector polarization and which has 180° alternations (parallel and antiparallel to y-axis) which match the periodic domain structure. In the far field region this alternating vector adds constructively at angles θ_n given by Sin $\theta_n = n \lambda/2d$ where d is the width of a domain, λ is the light beam wavelength, and n is the order of the beam (n = 0, 1, 3, 5 etc.). The maximum intensity in the diffracted beams is attained when the Faraday rotation is ±90°. In this special case 81% of the light

[1]Technical Report AFAL-TR-72-396 (March 1973)

[2]Technical Report AFAL-TR-74-183 (September 1974)

[3]Technical Report AFAL-TR-75-122 (August 1975)
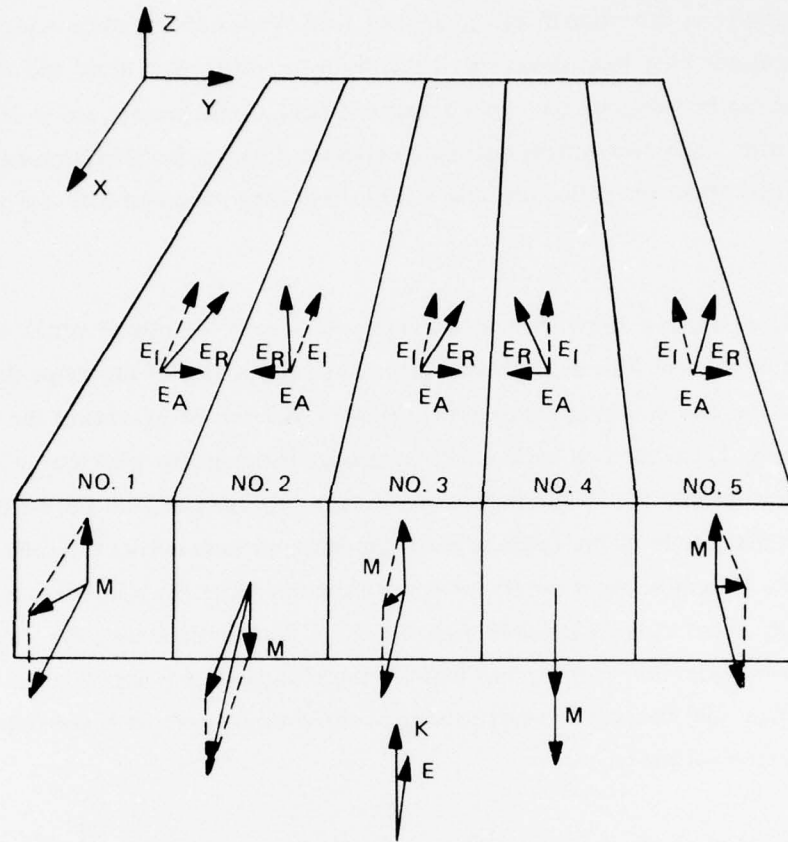
Figure 1. Stripe domains in a platelet. One component of magnetization, M, points out of the plane in the odd-numbered domains and into the plane in the even-numbered domains. Light propagates upward with a wave vector K perpendicular to the platelet and is rotated clockwise (with respect to K) in even-numbered domains and counter clockwise in odd-numbered domains. The rotated optical electric vector is E_R; the initial is E_I, and the alternating component is E_A.

3

goes into the first order diffracted beams, 9% goes into the third order beam, and so on. Not only do the stripes line up parallel to an applied magnetic field but the stripe width depends inversely on the strength of the applied field. Variations in stripe width of an order of magnitude have been measured. Thus, both the diffraction angle and the diffraction direction can be varied by the applied magnetic field. Consequently, stripe domains can be used as a wide angle, two dimensional light deflector. Changes in diffraction angle of $20°$ and rotation about the deflection axis of $360°$ have been measured with a green (5145 Å) Ar laser line.

The rate at which a stripe domain deflector can scan is the rate at which the stripe domains can be altered. This depends on the intrinsic properties of the stripe domain element, and the rate at which the external magnetic fields used to control the stripes can be changed. There are two basic switching modes for magnetic platelets: wall motion and magnetization rotation. While the speeds of both processes depend on the materials used and the magnitude of the fields applied, the latter process occurs typically in approximately 10 nanoseconds, while the former process takes place in a few microseconds. While either mode is possible with the stripe domain deflector, the wall motion process appears preferable at this point because the electronics for applying the magnetic field are simpler, and because the extra speed of the rotation process is not required for the applications anticipated.

The efficiency of the deflector can be dramatically improved by using the high figure of merit garnets. The efficiency vs wavelength is shown for various materials in Figure 2. The original 1.06 μm material was YIG. The efficiency is about .14 at room temperature and about .8 for YIG at $77°$K. The value for YIG shown in Figure 2 is lower than this but reasonable since the efficiency depends on the exact location of the absorption band edge. The efficiency of $Gd_2 Bi Fe_5 O_{12}$ is over .8 for a broad range of wavelengths at room temperature. Furthermore, the high rotation allows the use of platelets which are about 300 μm thick for single pass operation and which are about 30 μm thick in multiple pass configuration. The efficiency of $Bi_{.7}Y_{2.3}Fe_5O_{12}$ is also quite high. It is expected that by increasing the bismuth content, the efficiency can match that of the Gd garnet. Even at short wavelengths, 6328Å, the efficiency is at least 15%. Figure 2 also shows that $RbFeF_3$ possesses high efficiency over a large portion of the uv and visible spectrum.

4
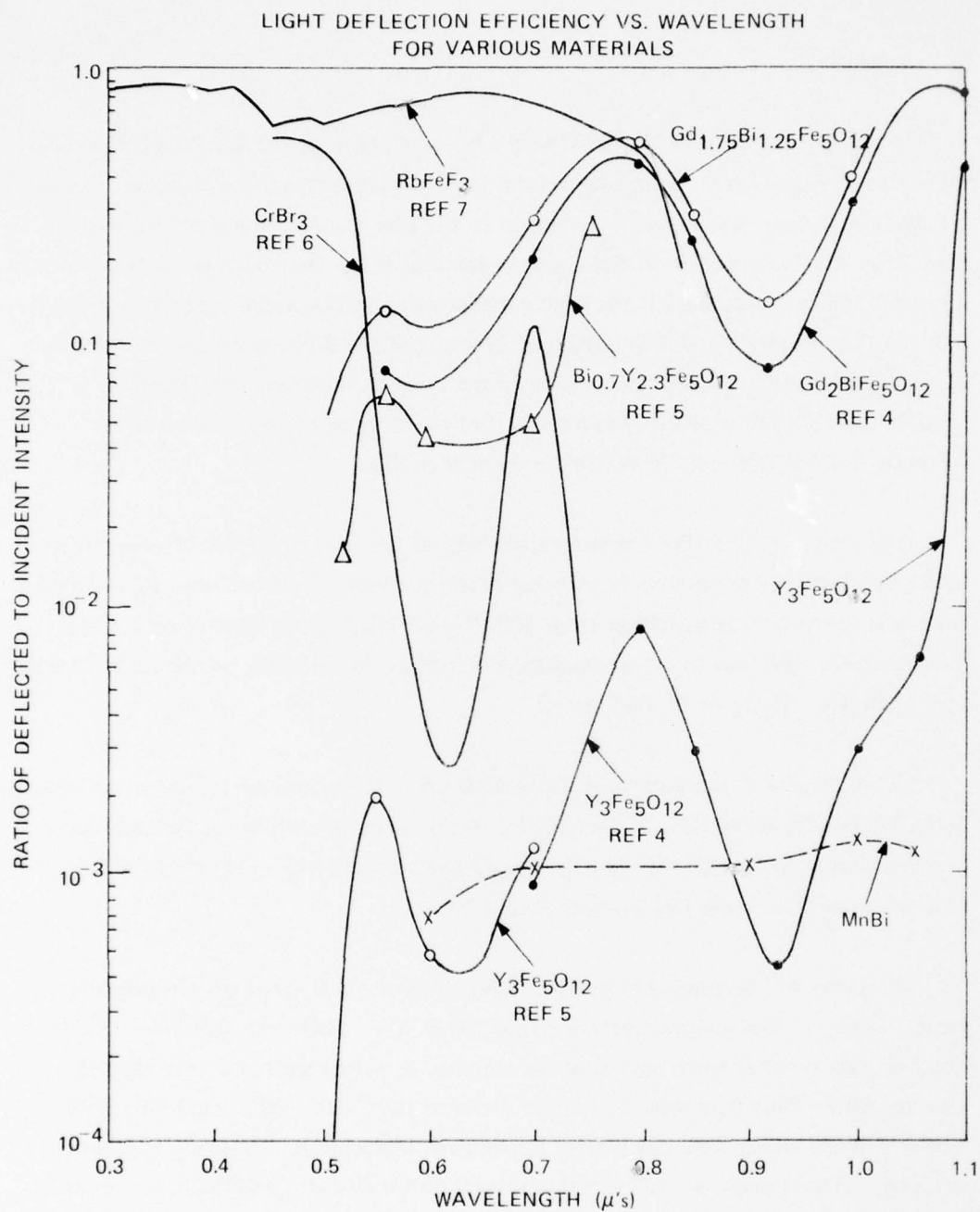
Figure 2. Light Deflection Efficiency vs. Wavelength for Various Materials
Computed Based on Data from References 4, 5, 6, and 7

5

SECTION II
GROWTH OF STRAIN-FREE BISMUTH GARNET CRYSTALS

A.   Summary

The main problem which existed with LPE of bismuth garnet crystal films on GGG substrates was that upon cooling the crystal from growth temperature to room temperature, a large tensile strain developed in the film plane.[3] This strain invariably resulted in the fracturing of all but the very thinnest films. Our measurements of thermal mismatch indicated (at least at the time corresponding to the beginning of this project) that the thermal strain could be explained in terms of the difference between the film thermal expansion coeffecient and the substrate thermal expansion coefficient. It is possible for a film to grow in compression, but the amount of compressive strain evidently was not adequate to offset the thermal strain.

It was assumed that the thermal expansivity of the film could not be easily altered. So we approached the problem of growing strain-free bismuth garnet films by attempting to reduce the growth temperature from $1000°C$ to $\sim 600°C$ and thereby reduce the thermal strain. This was to be accomplished by using a low melting temperature solvent, such as $Bi_2O_3 - B_2O_3$ or $Bi_2O_3 - Na_2O$.

In the process of working with the various low temperature melts, it became evident that certain melts allow enough compressive strain during growth to compensate for thermal mismatch. Specifically, $Bi_2O_3 - Na_2O$ melts and $Bi_2O_3 - PbO$ melts each produce strain-free, crack-free bismuth garnet crystals.

The melts will be presented in the following order: 1) Bi_2O_3 high temperature garnet, 2) Bi_2O_3 low temperature non-garnet, 3) $Bi_2O_3 - PbO$, and 4) $Bi_2O_3 - Na_2O$. The first two types of melts represent the simplest Bi garnet melt and were used in previous work. Thus they were reasonable melts to start with. The second two melts represent melts which were devised for low growth temperature. These melts produced strain-free films. Finally we will mention several different melts which did not produce

---

[3]Air Force Technical Report AFAL-TR-75-122 (August 1975)

useful films. Two x-ray techniques were applied to the analysis of films from these melts. The first is in-plane lattice match measurement, the second, thermal expansion measurement.

B. Bi_2O_3 Melts

The simplest lead free flux is Bi_2O_3. Other lead free fluxes have in addition BaO, B_2O_3. These lead-free fluxes are more difficult to work with than lead oxide fluxes; flux adhesion is a greater problem. Film cracking occurs due to adhesion and to differential expansion. Also, Bi_2O_3 has such a tendency to dissolve platinum that for some melts platinum crystals grow at nearly the same rate as garnet crystals. As noted by other investigators, the lower the melt temperature during deposition (the greater the supersaturation), the greater the percentage of bismuth in the resulting crystal.[8,9] The larger percentage of bismuth, the larger the lattice constant. As shown below, the lattice constant of crystals grown in Bi_2O_3 fluxes is such a strong function of growth temperature that very accurate temperature control is necessary to obtain growth in region I (defined as the region in which the in-plane lattice of film and substrate are the same).[10,11,12] In order to determine whether a film has been grown in region I or II (defined as the region in which the in-plane lattice constants of film and substrate are different[10,11]), it is necessary to measure the in-plane lattice mismatch between film and substrate, $\Delta a^{\parallel}$, with x-rays. The measurement of the perpendicular lattice mismatch, $\Delta a^{\perp}$, is not sufficient.

Melt 108, Table 1, is a high temperature Bi_2O_3 melt in which the principal precipitate is garnet. Figure 3 shows the perpendicular and in-plane lattice mismatches, $\Delta a^{\perp}$ and $\Delta a^{\parallel}$, between film and GGG substrate as a function of growth temperature for (111) films from this melt. Note that the in-plane mismatch is nearly zero in the region between $1050°C$ and $1070°C$. This constitutes region I. Above that region, films grow with such a deficiency of bismuth that the crystals grow with an in-plane lattice smaller than that of

[8]A. Akselrad, R. E. Novak, D. L. Patterson, A.I.P. Conf. Proc. 18, 949-953, (1973)

[9]S. Witterock, J. M. Robertson, T. J. A. Popma, P. F. Bongers, A.I.P. Conf. Proc. 10, 1418 (1972)

[10]P. Besser, et al, A.I.P. Conf. Proc. 5, 125-9 (1971)

[11]P. Besser, et al, Mat. Res. Bull. 6, 1111, (1971)

[12]H. Makino, et al, A.I.P. Conf. Proc. 18, 80, (1973)

TABLE 1. Bi GARNET MELTS

Concentrations in millimoles

Melt	108	42B	150	151	161D	163
Bi_2O_3	107	186	96	190	241	215
$Pb\,O$	–	–	477	954	–	–
Ga_2O_3	–	–	–	15	5.3	–
Fe_2O_3	20–60	27	58	102	53	49
Yb_2O_3	3–5	4.3	1.5	–	5.11	5.2
Tm_2O_3	–	–	–	3	–	–
Al_2O_3	–	–	–	–	–	3.2
Na_2O	–	–	–	–	9.6	8.5

8

the substrate, rather than supporting the high tensile strain of an in-plane match. The resulting lattice imperfections make the magnetic properties of such region II films unsuitable. Likewise, films grown at temperatures lower than 1050°C have such a surplus of bismuth substitution that films grow with in-plane lattice larger than that of the substrate, rather than supporting the high compressive stress of region I growth.

Lattice parameter difference measurements were made by diffraction with a Kα copper x-ray beam. Rocking curves were taken for the (8,8,8), (0,8,8), (4,6,6), (12,8,0), and (12,6,0) diffraction planes. The difference in diffraction angles for each diffraction plane gives a linear relation between the in-plane and normal lattice mismatches.[12]

Note that, with the exception of one borderline data point, all the films in Figure 3 have a smaller lattice in the direction normal to the substrate than parallel to the plane. This means that at room temperature, where the data was taken, all the films are under tension. This occurs because the coefficient of expansion of the film is larger than that of the substrate.

Figure 4 shows $\Delta a^{\perp}$ vs. temperature for two films from melt 108. The thermal expansion measurements were taken by mounting a modified Ungar #4035 Heating Unit on the Nonius eucentric goniometer. The differential thermal expansion coefficient can be computed from these curves. $\Delta\alpha = \dfrac{\Delta a(T_1) - \Delta a(T_2)}{(T_1 - T_2)\,a}$ where T_1 and T_2 are temperatures. This large differential expansion coefficient causes all melt A films to be under tension at room temperature, even films grown at the compressive limit of region I. The films in figure 4 were grown in region I and show a differential coefficient of expansion, $\Delta\alpha$, of $3.3 \times 10^{-6}/°K$ in the range from 23° to 500°C. The corresponding value for YIG on GGG is $2.0 \times 10^{-6}/°K$ in the same range, based on the work of Geller et al.[13] The $\Delta\alpha$ for the melt 108 films over the temperature range $23°C \leq T \leq 1060°C$ can be estimated by adding the strain limit of Makino et al[11] at the lower end of region I to the observed Δa at room temperature of 0.018 Å; the result is $\Delta\alpha \approx 3 \times 10^{-6}/°K$ over the region $23°C$ T $1060°C$. The corresponding difference between bulk YIG crystals over the same temperature range is $1.25 \times 10^{-6}/°K$.[12] At the time of this writing, it is not established whether the higher differential dilation of the L.P.E. films as opposed to that of the bulk crystals is due to the added bismuth. However, the difference in

---

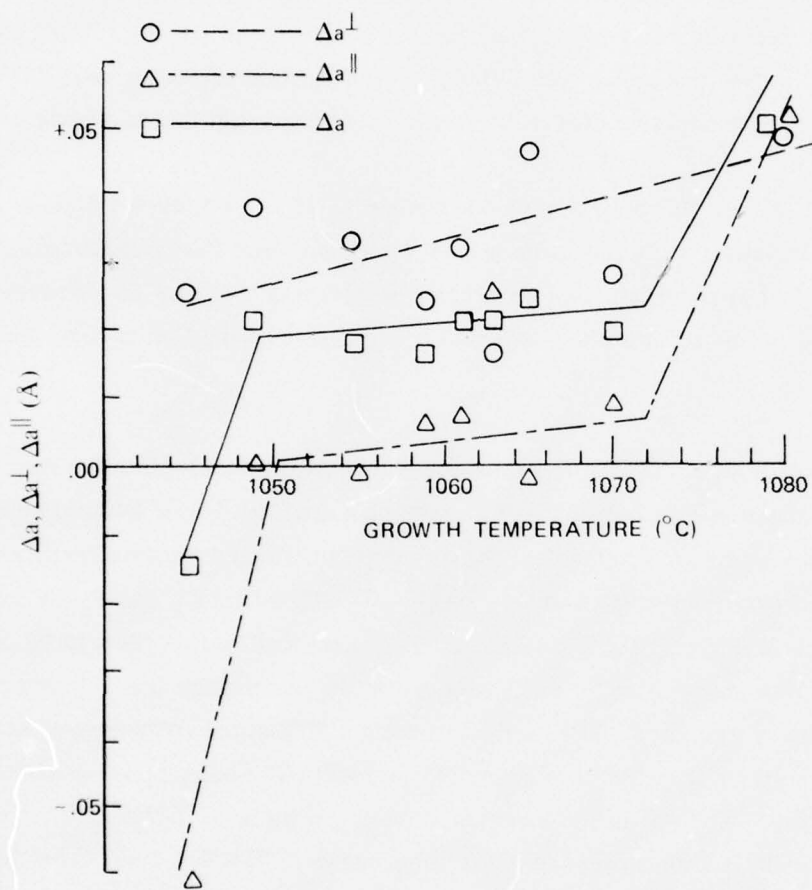[13] S. Geller, et al, Mat. Res. Bull. 7, 1219 (1972)
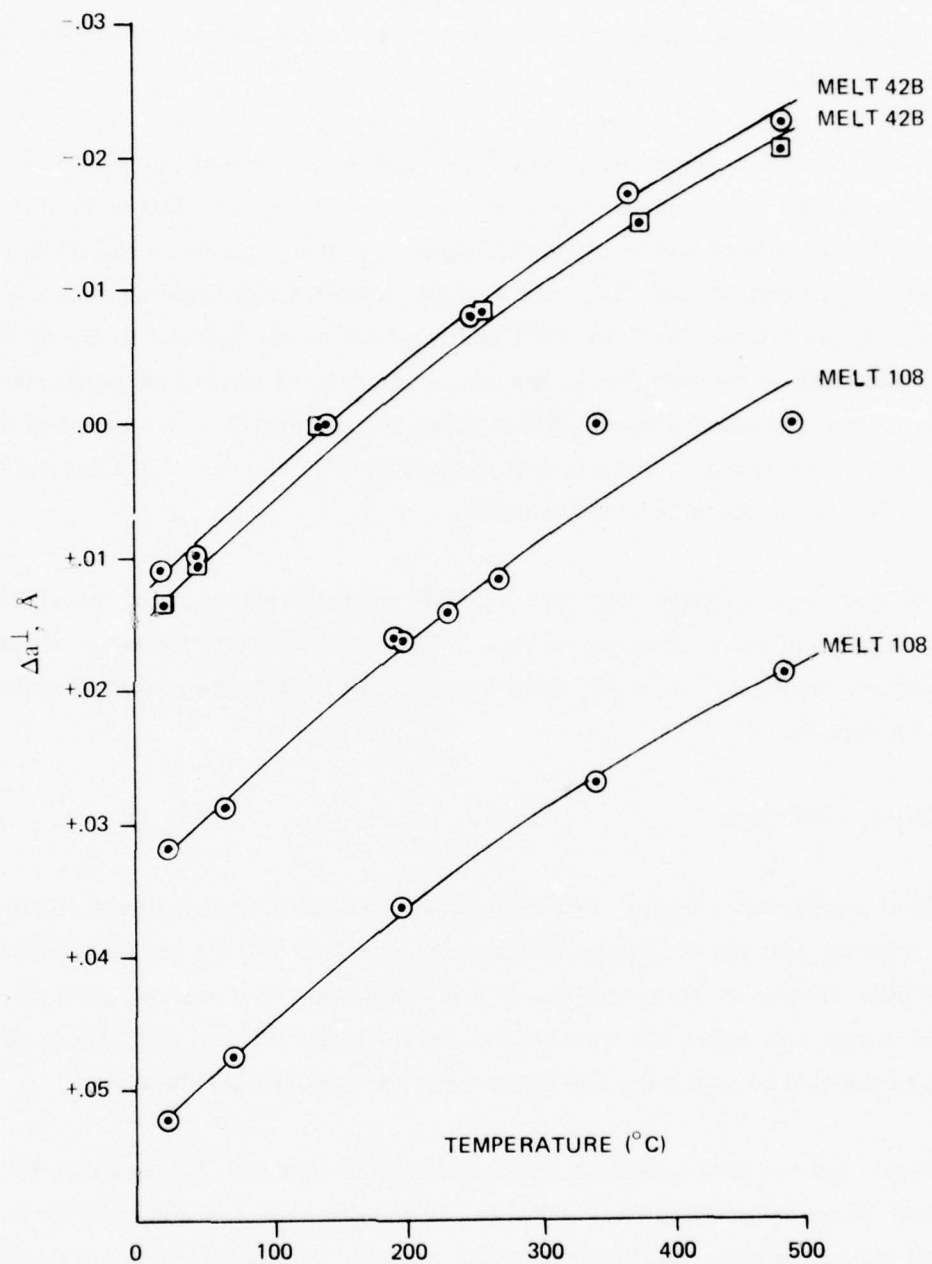
Figure 3. Lattice Match Bi$_2$O$_3$ Melt

10

Figure 4. $\Delta a^\perp$ vs. Temperature

11

coefficient of expansion between film and substrate is large enough to crack the films, provided the film thickness exceeds one micron, and indeed all the films in Figure 3 are cracked. Uncracked melt 108 films ranging in thickness from 10 to 30 microns were grown previously on elastically deformable GGG substrates thinned to 10 microns by Syton polishing and phosphoric etching.

In order to overcome the thermal cracking problem, a low temperature melt was sought to decrease the excursion from growth to room temperature. This melt, melt 42B of Table 1, has a low enough saturation temperature so that crack-free region I films were obtained. Curves of $\Delta a^{\perp}$, $\Delta a^{\parallel}$, and Δa versus growth temperature are shown in Figure 5. Region I spans 765°C to 785°C and is limited on the high end by the saturation temperature. Films grown at the low temperature end of region I are nearly strain free at room temperature. Thermal dilation curves for two melt B films are plotted in Figure 4; they are similar to those of melt A films. For the two melt 42B films $\Delta\alpha = 3.50$ x 10^{-6}/°K over the range $23°C \leqslant T \leqslant 500°C$.

The principal precipitate from melt 42B is an unidentified non-garnet crystal. The thickness of L.P.E. garnet films grown in melt 42B is limited by the formation of this precipitate in the melt. Thus Bi_2O_3 melts do not lend themselves to growth of strain-free deflector crystals.

C. Bi_2O_3 – PbO Melts

Next a sequence of Bi_2O_3 – PbO melts were investigated. Melts 150 and 151 of Table 1 are the two which represent the end members: Melt 150 is a (Bi Tm) (Fe Ga) garnet melt. The size of Tm is such that at a Bi substitution level near one atom per formula a pure iron garnet film would not match the lattice constant of GGG. So Ga was added to the melt to reduce the film lattice. Melt 151 is of the BiYbIG type.

Figure 6 shows lattice constant data for films from melt 150. The data is badly scattered. Nevertheless the interval 700°C to 750°C is included in region I, and in this interval some films are strained compressively. Actually, the films themselves were of poor uniformity which explains some of the scatter in Figure 6. The thermal mismatch measured for two melt C films is 1.7×10^{-6}/°K and 2.26×10^{-6}/°K in the 23°C to 500°C range.
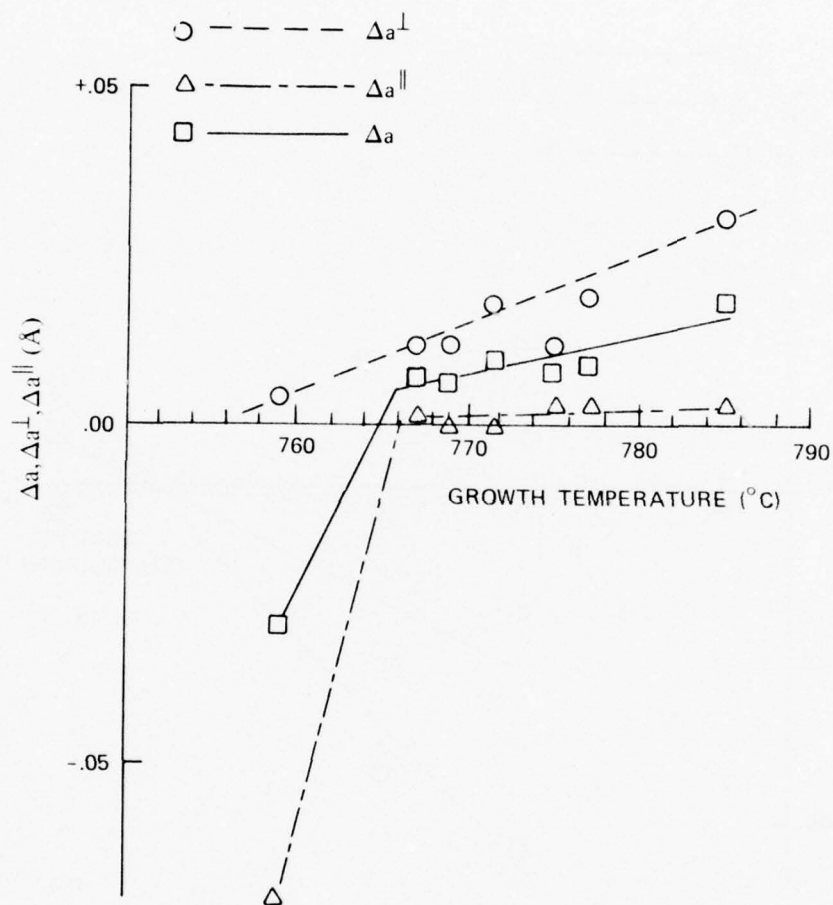
12

Figure 5. Δa, $\Delta a^{\perp}$, $\Delta a^{\parallel}$ vs. Growth Temperature Melt 42B
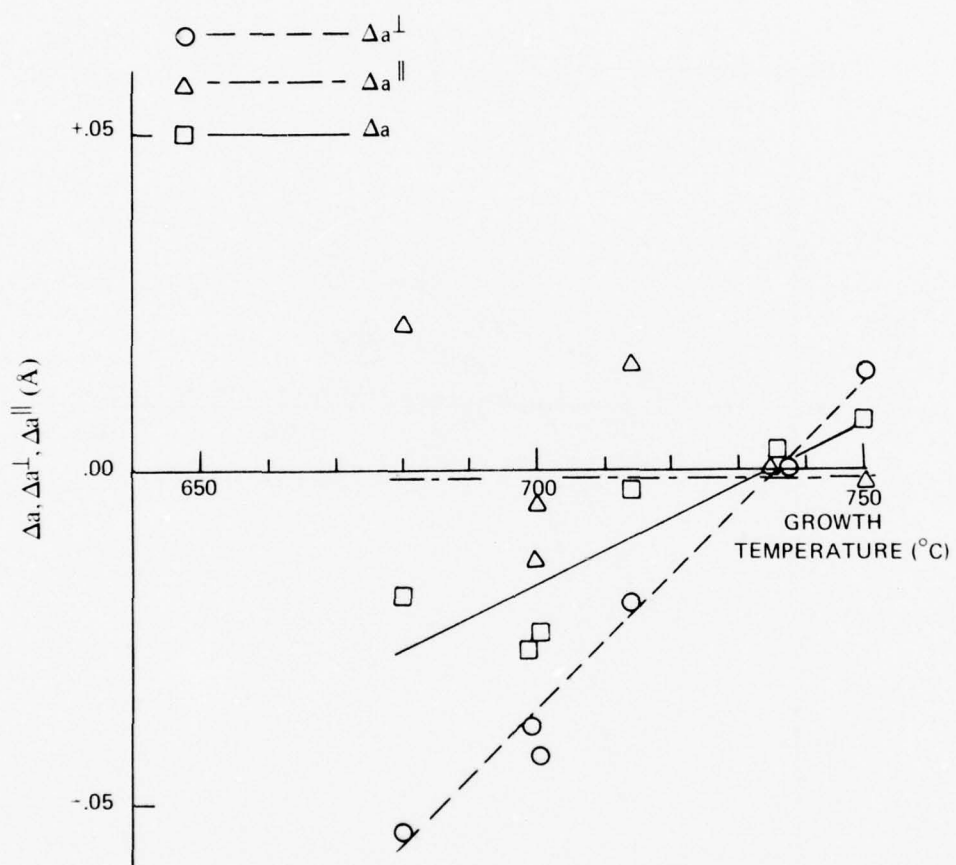
13

Figure 6. Δa vs. Temperature Growth Melt 150

14

Figure 7 shows lattice constant data for melt 151 films. Region I includes 700°C to 730°C. At the low temperature end, the films are nearly strain-free. Thermal mismatch data for two melt 151 films are $\Delta\alpha = 2.82$ and $3.14 \times 10^{-6}/°K$.

Thus the low temperature Bi_2O_3 – PbO melts do produce strain free films. Flux adhesion, when it occurs with these melts, does not seem to damage the film.

D.   Bismuth Ionic Na_2O Melts

Several solvents could be mixed with Bi_2O_3 to make a low temperature melt. The systems of Bi_2O_3 – Na_2O and Bi_2O_3 – K_2O were examined in detail.

Figure 8 shows the liquidus curve obtained for Bi_2O_3 – Na_2O, and Figure 9 shows a similar curve for Bi_2O_3 – K_2O. In each curve there is a low temperature region, 500°C to 600°C for ionic oxide concentrations of .2 to .3. So the bismuth ionic mixture ought to be a useful low temperature solvent. A comparison of ionic radii [14] is given in Table 2.

TABLE 2

	VIII	XII
K^+	1.65 Å	1.74 Å
Ba^{++}	1.56 Å	1.74 Å
Pb^{++}	1.45 Å	1.63 Å
Na^+	1.30 Å	–
Bi^{+++}	1.25 Å	–

Since the sodium radius is intermediate to Bi^{+++} and Pb^{++}, it is entirely possible for Na^+ to substitute into the garnet lattice. The radius of K^+, on the other hand, is larger than that of Ba^{++}; and the larger Ba^{++} ion does not substitute into the garnet lattice.

The experimental results with the bismuth ionic melts are that strain free BiYbFeGa garnet and BiYbFeAl garnet crystals can be grown in Bi_2O_3 – .04 Na_2O melts. Films of BiYbFe and BiLuFe garnet can be grown only with difficulty in the Bi_2O_3 – K_2O system.

---

[14]Shannon and Pruitt

15
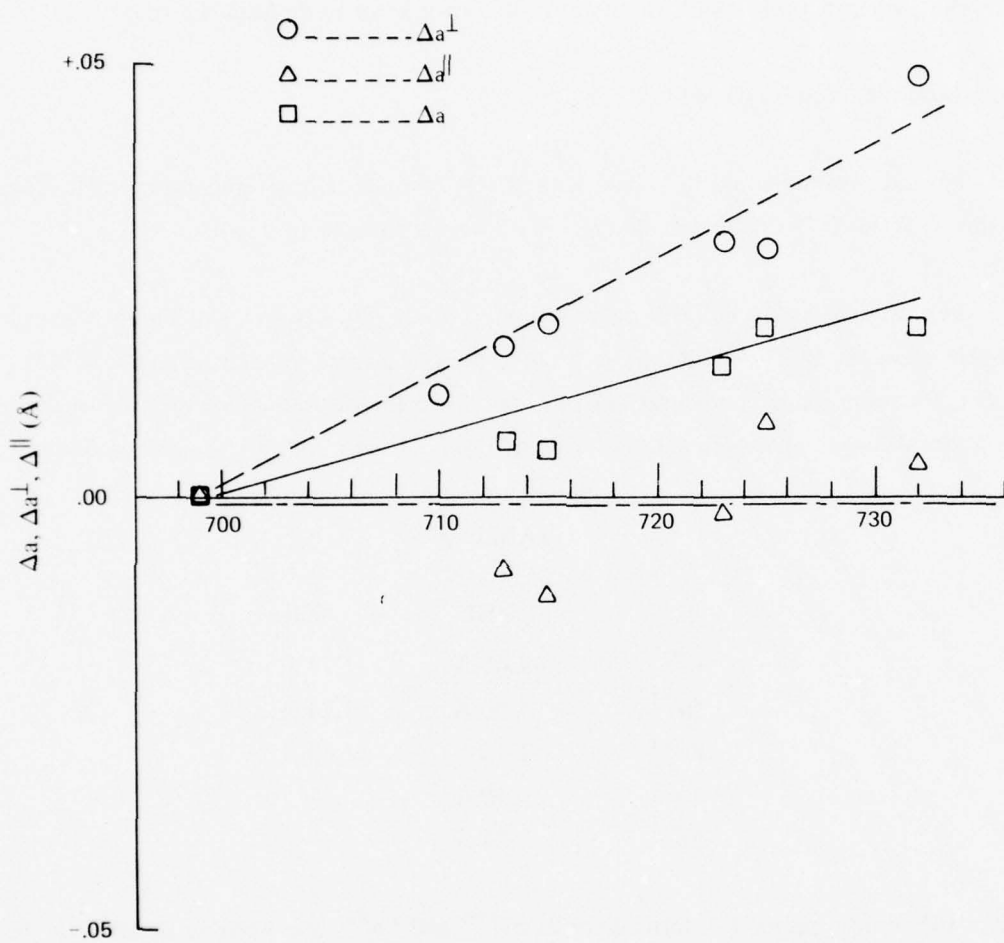
Figure 7. Δa vs. Growth Temperature Melt 151D

16
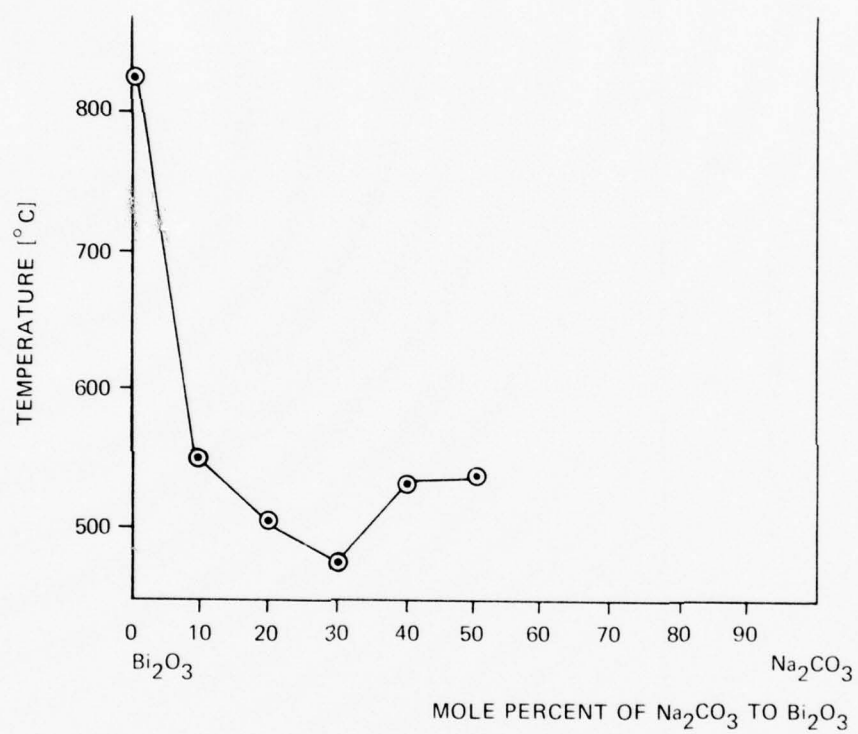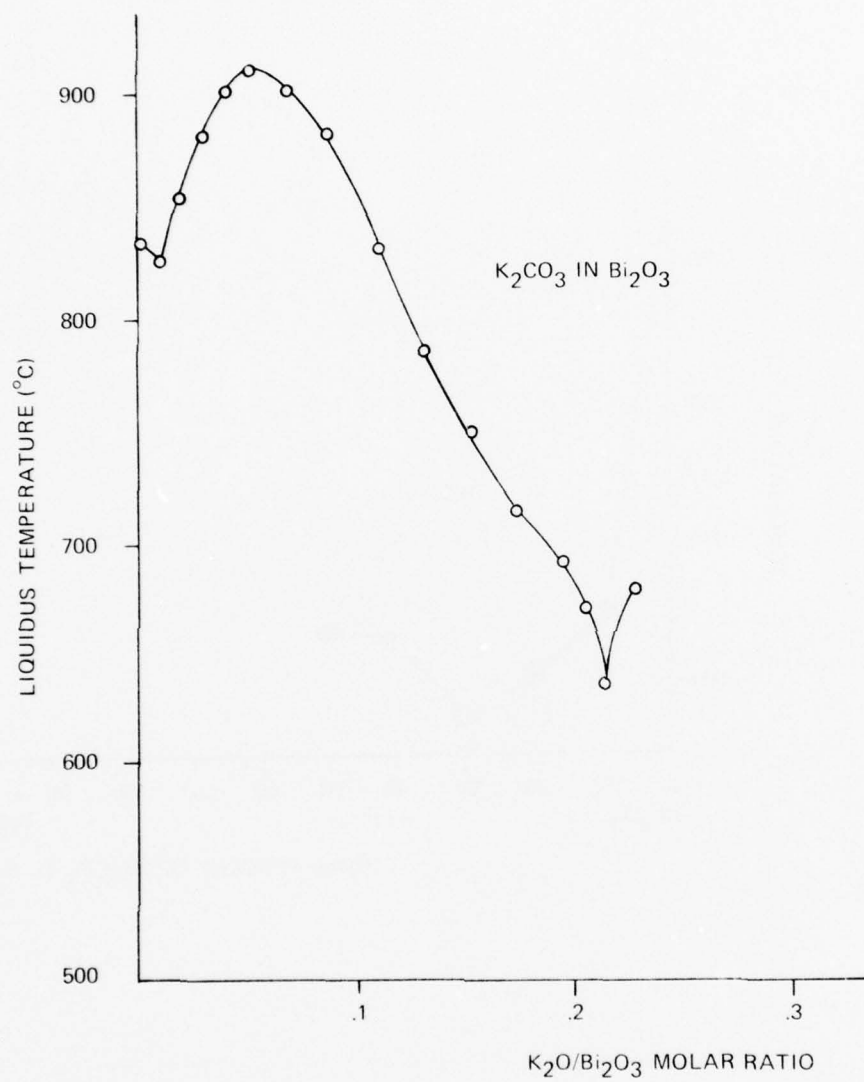
Figure 8.   Liquidus Na$_2$ – Bi$_2$O$_3$

17

Figure 9. Liquidus Temperature vs K_2O/Bi_2O_3 Ratio

18

The lattice constant data for BiYbFeGa films from the Bi_2O_3 -0.04 Na_2O melt 161D is shown in Figure 10. Region I includes all of the films. It is clear that strain-free as well as compressively strained crystals were grown in this system. Note that the strain-free growth temperature is 864°C. Melts 42B and 151D produced strain-free crystals only at the extreme edge of Region I and at temperatures well below 864°C: 765°C for melt 42B, and 700°C for melt 151D.

The thermal mismatch data for two melt 161D films is $\Delta\alpha$ = 3.99 and 5.44 x $10^{-6}/°K$. These values exceed the $\Delta\alpha$ values for melt 42B and 151. Thus, whether or not a crystal is strained at room temperature is determined by the composition of the melt as much as the thermal mismatch and growth temperature. Apparently a crystal film growing in a Bi_2O_3 - Na_2O melt can support more compressive strain while maintaining $\Delta a^{\parallel}$ = 0. Another way of saying this is: as the compressive strain of a growing film becomes larger and larger, it is energetically more difficult for an atom to be bonded to the film as opposed to being in the melt. Na_2O when added to the Bi_2O_3 melt tends to make the state of being bonded to the growing film energetically more favorable. This result can probably be generalized to include Bi_2O_3 - PbO melts. Furthermore, it probably applies to other crystal growth systems as well.

The Bi_2O_3 - Na_2O system worked best at only 4% Na_2O. Greater amounts of Na_2O made the garnet phase less stable. Several other crystal types percipitate outside of the very narrow garnet region. Attempts to identify the crystals were unsuccessful since absolutely no peaks showed up in powder diffraction measurements. Precipitate crystals of similar color and habit turned up in the Bi_2O_3 - K_2O system, and in several other systems. Flux adhesion occured in the Bi_2O_3 - Na_2O melt, but did not seem to damage the film to any extent.

In summary, strain-free, crack-free Bi garnet films were obtained from Bi_2O_3 - Na_2O and Bi_2O_3 - PbO melts. The details of melt composition are as important as the growth temperature and thermal mismatch.

Melts of Bi_2O_3 - B_2O_3 - Na_2O, Bi_2O_3 - BaO, and Bi_2O_3 - BaO - V_2O_5 were tested for BiYbIG crystal growth. Multiple phases often occurred and whenever the garnet phase did occur it was stable only over a very narrow range. Compared to Bi_2O_3 - Na_2O and Bi_2O_3 - PbO these other melts are not suited for deflector crystal preparation.

19
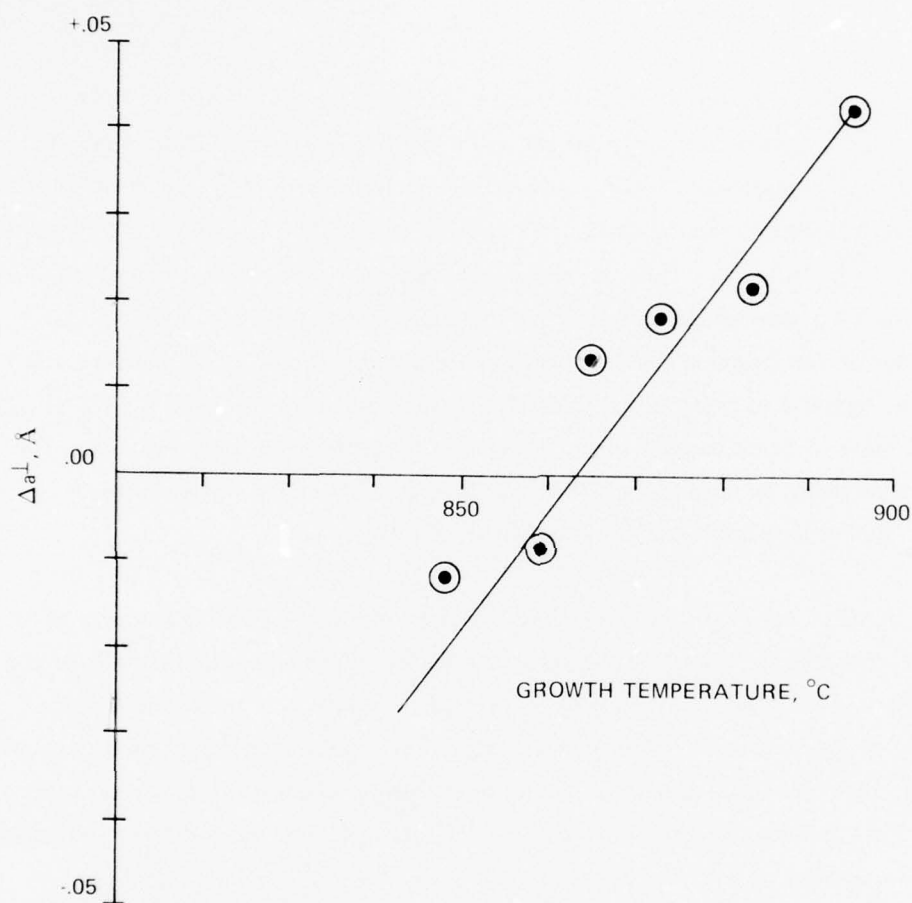
Figure 10. $\Delta a^{\perp}$ vs. Growth Temperature, Melt 161D

20

E.   Other Bi_2O_3 Melts

The $Bi_2O_3 \cdot B_2O_3$ system was investigated for BiYbIG LPE. The $Bi_2O_3 - B_2O_3$ system consists of a series of 5 eutectics,[15] the first of which occurs at 622°C. (See Level et al Phase Diag. For Ceramists Fig. 323.) Thus it was hoped that 1) a low growth temperature of 700 - 800°C could be obtained and 2) in-plane match could be achieved over a convenient temperature range, eg. 25°C.

The method is to add B_2O_3 to a Bi_2O_3 garnet melt, and then add Yb_2O_3 to bring the melt back to a garnet phase. The results can be summarized: a base or starting melt of 135 mm Bi_2O_3, 51.5 mm Fe_2O_3, and 4.5 mm Yb_2O_3 produced garnet crystals at 970°C. To this melt B_2O_3 and Yb_2O_3 were added in stages so that the final melt is 135 mm Bi_2O_3, 28.72 mm B_2O_3, 51.5 mm Fe_2O_3, and 11.5 mm Yb_2O_3. Crystallites grown at 949°C were x-rayed and found to have a lattice constant of 12.360. Thus, the crystal contains $\sim$ .8 Bi per formula.

The main features of this system are 1) reduced growth temperature for a given amount of bismuth substitution, 2) increased flux adhesion due to the glassy nature of the flux. This system does not appear to offer any substantial advantage.

---

[15] Levine and McMurdie, Phase Diagrams for Ceramists, Amer. Cer. Soc. 1964, Fig. 323.

SECTION III
CRYSTAL CHARACTERIZATION SUMMARY

A. Measurement of Magneto-Optic Variables

Data on Faraday rotation, F; absorption, B; thickness; magnetic moment, $4\pi M$, and anistropy, H_k were obtained for Bi garnet crystals from five different types of melts — Table 1. The crystals and the melts used for the growth of these crystals form an evolutionary sequence which were intended primarily to show experimentally how to obtain unfractured and strain-free light deflector crystals. The melts and crystals, as such, are not sufficient to constitute the complete set of crystals necessary to specify the relationships between $4\pi M$, H_k, F, B, and bismuth content. Thus, magneto-optic data represents progress made toward developing the bismuth garnet crystals for beam steering. The most important quantities are F and B since the bismuth substitution is intended to increase the Faraday rotation but not the absorption. In order to get specific rotation, (deg/cm), and absorption, (db/cm), the crystal thickness must be measured. This is done by interferometry by utilizing the index of refraction discontinuity at the crystal substrate interface. Interference data is obtained by visual microscopy or alternatively by Beckman DKII Spectrograph plots.

B. 1.06 μm Magneto-Optic Effects

The measured Faraday rotation of several bismuth Ytterbium iron garnet crystals is shown in Table 3.

TABLE 3. 1.06 μm FARADAY ROTATION

Melt	Type	Crystal	F deg/cm
163	BiNaAl	1048	3294
163	BiNaAl	1050	1894
163	BiNaAl	1052	3418
161D	BiNaGa	109	1584
151	BiPb0	1014	2128
151	BiPb0	1020	1476

22

Two crystals in the NaAl group have $F > 3000°/cm$ which is the goal for bismuth garnets grown on GGG substrates. Lattice match and $4\pi M$ measurements of the NaAl containing crystals indicate the large rotations are probably due to their enhanced bismuth concentration which exceeds one atom per formula compared to .8 atoms per formula for the rest of the crystals in Table 3. The dependence of F on sodium which may be in the crystals and aluminum which is in crystals 1048, 1050, and 1052 is not known. Aluminum substitution ought to reduce F. The variation in F from crystal to crystal is due partly to measurement error in determining the amount of rotation of the laser beam as it passes through the crystal and the crystal thickness error. The 1.06 μm optical absorption, B, of crystal 1048 and 1052 is not accurate because their surfaces are not of sufficient optical quality. Large values of F at 1.06 μm ought to be consistent with low absorption at this wavelength.

The most interesting part of the spectrum for garnet magneto-optic application includes the 1 μm region. Magnetic garnets have an optical transmission window from 1 μm to 7 μm wavelength which includes several laser wavelengths. For example, Nd YAG lases at 1.06 μm, and He-Ne lases at 1.15 μm. The 1.06 μm absorption coefficient of BiGdIG bulk crystals has been reported to be as low as 10 db/cm.[4] So when the low absorption is combined with the large, 3000°/cm Faraday rotation, magneto-optic efficiencies of 300°/db should be possible. This is equivalent to a 0.3 db insertion loss with 90° rotation. Absorptions of even 100 db/cm are acceptable: 90° of rotation results in 3 db insertion loss. We have discovered the 1.06 μm absorption coefficients of epitaxial Bi-garnet crystals are higher than the 10 db/cm bulk value. Absorption coefficients of 100 to 1000 db/cm at 1.06 μm were measured. Accordingly we have sought an explanation of 1.06 μm absorption based on the band theory of semiconductor solids.

Iron garnets typically have a band gap of 2 - 3 ev as evidenced by the strong absorption band at 5000 Å wavelength, and have valence 3 + cations. Monovalent or divalent cation impurities such as Ca++, Pb++ create acceptor states whereas tetravalent or pentavalent cation such as Si^{4+} create donor state. Oxygen vacancies create donor states. Several experiments were performed 1) Seebeck measurement to establish majority carrier type and conductivity vs temperature; 2) annealing in oxygen to remove oxygen vacancies, 3) resistivity and absorption versus temperature was measured. In addition, chemical impurity analysis measurements via spectroscopy and electron microprobe were initiated.

23

The main purpose of the Seebeck measurement is to establish the majority carrier type for each film. This in turn can be used to verify the chemical impurity measurement. In particular, oxygen vacancies cannot be measured directly, but Seebeck measurements combined with oxygen atmosphere annealing indicates the extent of oxygen vacancies. The majority carrier measurement can also be used to determine the presence of pentavalent bismuth, Bi^{5+}, which would be a donor. The Seebeck voltage measurement was performed by heating one of two electrical contacts on the film by light focused from a 500 W tungsten bulb. The voltage produced by migration of majority carries in the thermal gradient between the contacts was measured with a Keithly 610 electrometer. The contacts were liquid InGa solder which was prepared by melting the two metals on a hot plate.

A simple system was developed for annealing garnet films. A tube furnace was used with a tube 2½ feet long and 1¼ inch in diameter with an active heating length of approximately 6 inches. The temperature of the oven was stabilized before the garnet film samples were inserted. The garnet films were placed on small platinum boats which were slowly moved along the tube to the active furnace section. Insertion and removal time were 15 to 30 minutes to minimize thermal stresses. For atmosphere control a loosely fitted plug with an input gas line was applied to one end of the furnace tube. The other end of the furnace tube was fitted with a baffle to smooth the gas flow.

The results of annealing three crystals in oxygen are presented in Table 4. Only in crystal 109 is there a slight shift from n to p type. Thus oxygen vacancies which are removed by annealing do not dominate the electrical type. The annealing was accompanied by a reduction in absorption coefficient in 1008 and 109. However, the final absorption is very large compared to what is required. Evidently oxygen vacancies do not dominate the absorption process.

Chemical analysis revealed amounts of Ca in both the crystals and starting material, and we were unable to remove it by hydroxide reaction precipitate techniques. Crystal 117 is a duplicate of 1014 except that it was grown in a high purity melt in which the starting materials are 99.99999 pure. Unexpectedly, the absorption of crystal 117 is more than twice that of 1014, Table 5. Thus, low absorption requires more than starting material purity.

24

TABLE 4. ANNEALING EXPERIMENT

Crystal	$\frac{\Delta B}{B}$	Unannealed	Annealed
		— Type —	
1008	-.50	0	0
109	-.26	n	0
1052	0	p	p

TABLE 5

Crystal	B (db/cm)	ρ (Ω cm)
1008	100	6×10^9
1014	496	4×10^{10}
117	1616	4×10^8
102	1749	1×10^5
109	679	3×10^5
1052	4542	1×10^6

The measurement of resistivity for various crystals is shown in Table 5. We may expect that absorption would correlate with resistivity. Undoped or perfectly compensated crystals ought to have low absorption and higher resistivity. However, this pattern is not evident. While crystal 1014 has the second lowest absorption and highest resistivity, crystal 109 has the third lowest absorption but the second highest resistivity.

The absorption coefficient values are somewhat uncertain. They depend on accurate measurement of the incident, reflected, and transmitted power and film quality. The situation is complicated by the absorption losses which occur while the light undergoes multiple reflections inside the film. The multiple reflections are a result of the film air interface and the film substrate interface. If the index of refraction is known for each medium, then transmitted fraction, T, is given by:

$$T = \frac{(1 - R)^2 \, e^{-\beta x}}{1 - R^2 \, e^{-2\beta x}}$$

where

$$R = \frac{(n_1 - n_2)^2}{(n_1 + n_2)^2}$$

Measurement of n_2 by Brewster's angle as determined by the polarization method shows that the film index varies from film to film. Furthermore, the film thickness must be measured precisely. This is done by interference but requires knowledge of the index of refraction. For these values of T, we have used $R = .14$ or measured the reflected intensity. The general result, that at least some of the crystals have absorption coefficients near or below a useful value of 100 db/cm, will be unaffected by better absorption measurements.

In the process of measuring resistivity, the photo-conductivity of each film was checked. In the case of GGG substrate crystals, the photo response was strong. However, no film exhibited photo-conductivity. From this we conclude that the electronic transitions which causes absorption are ones with non-conducting or localized final states, such as excitons.

The variation of resistivity with temperature was measured for several crystals. Low temperature measurements were achieved by cooling the crystal in a Cryogenic Technology cooler. High temperature measurements were obtained via a hot plate. The resistivity versus temperature curves are those of compensated semiconductors with an extrinsic region at low temperatures, $T < 100°K$. Figure 11 shows P vs T^{-1} for crystal 109. At the same time absorption versus temperature was measured vs T. The resistivity changes by 6 orders of magnitude with activation energies of .31 ev and .54 ev. The absorption is temperature independent. Therefore, absorption is not proportional to the conductivity. So, the absorption process does not involve transitions between two conduction band states. The large variation of resistivity indicates that the donors and acceptors are not close to the band edges. In crystal 109 the number of conduction carriers varies rapidly with temperature. The possibility for localized, band gap state transitions does exist. The complete treatment of band gap state transitions requires chemical impurity data which are not available and analysis of structural defect states. Complete transmission spectra were obtained with a Beckman DKII instrument. The transmission is featureless above the band edge for all of the crystals examined. Figure 12 shows the transmission curve for crystal 148.
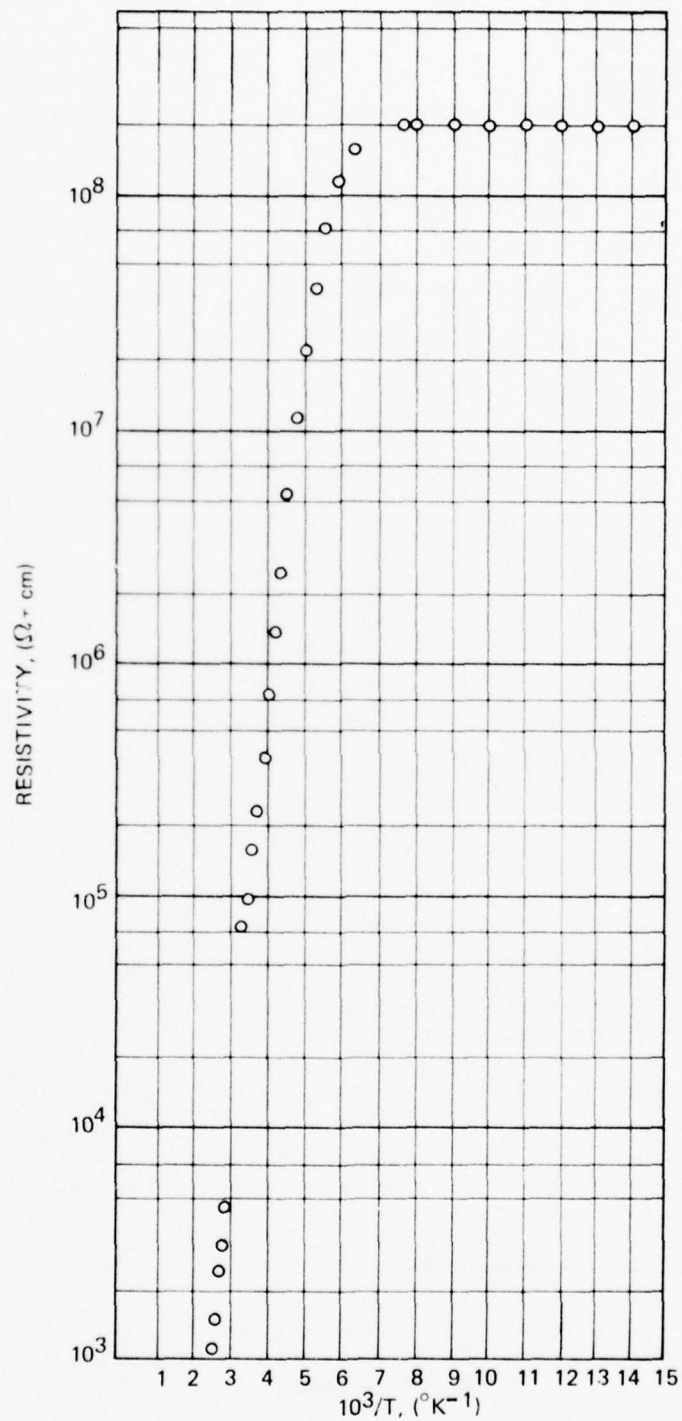
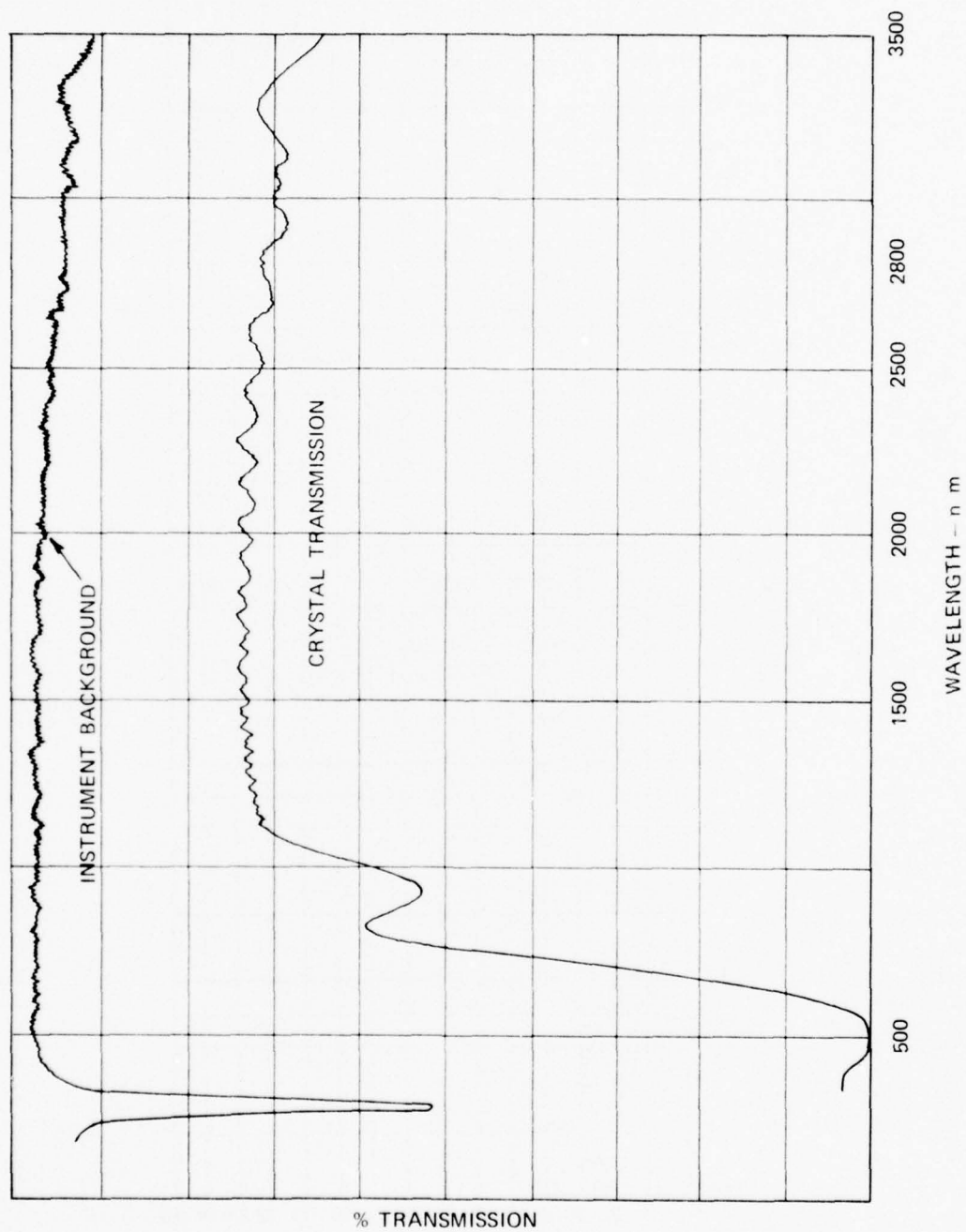Figure 11. Resistivity vs Reciprocal Temperature of Crystal 109

27

Figure 12. Transmission vs. Wavelength Crystal 148

To summarize the investigation of the optical absorption mechanism, the most probable cause is electronic transitions among localized states in the band gap. Further treatment is required to fully understand the origins of absorption.

The most recently grown crystals are BiLuIG on GGG substrates. Lu was chosen because it is the smallest rare earth and so more Bi can be substituted into the crystal and because Lu invariably is a trivalent cation. (Yb can be either divalent or trivalent). Several of the twenty-five crystals prepared from a Bi_2O_3 – PbO melt similar to 151 have absorption coefficients near 100 db/cm and several crystals appear so transparent that the absorption could not be measured. Table 6 gives absorption together with Seebeck voltage and resistivity for the BiLuIG crystals. At the time of this writing we are obtaining microprobe chemical analysis to determine whether the variation of absorption is due to impurities.

C.   6328 Å Faraday Rotation and Absorption

Table 7 shows F, B and F/B, the figure of merit for crystals of $(BiYb)_3$ $(FeGa)_5$ O_{12} from melt 150 and of $(BiYb)_3$ $(Fe)_5$ O_{12} from melt 151, both $Bi_2O_3 \cdot PbO$ melts. It also gives data for $(BiYb)_3$ $(FeGa)_5$ O_{12} from melt 161D and $(BiYb)_3$ $(FeAl)_5$ O_{12} from melt 163, both Bi_2O_3 – Na_2O melts at 6328 Å wavelength. The bismuth garnet crystals from melt 163 have the very large Faraday rotation desired. For comparison, the rotation of YIG is about $3000°/cm$. The rotation of film 1048 and 1052 is nearly ten times that of YIG. As in the case of 1.06 μm results, the BiYb FeAl G crystals have the largest Faraday rotation.

Of fundamental importance from an application point of view is the optical figure of merit $\frac{F}{B}$. Because there are four distinct compositional groups, the easiest way of

TABLE 6

SAMPLE	B 1.06 μm db/cm	Resistivity $\Omega - cm$	Type
133	1415	7.47×10^7	—
138	1410	—	n
140	24	1.7×10^{11}	p
141	41	6.4×10^{10}	p
142	440		p
144	40	1.1×10^{10}	p
145	71	8.3×10^{11}	p
147	39	2.3×10^7	p
148	259	4×10^{10}	p
149	100	2×10^{10}	p
150	100	8×10^8	n
151	218	1.1×10^9	p

TABLE 7. 6328 Å WAVELENGTH

MELT	CRYSTAL	F	B	F/B
150	1003	3623	7920	.46
	1004	5714	7194	.79
$(BiYb)_3 (FeGa)_5 O_{12}$	1005	1894	8131	.23
	1006	5556	8372	.67
Bi_2O_3PbO Melt	1007	8160	7976	1.02
	1008	7610	7053	1.06
	1015	6071	7470	.81
151D	1009	1984	4958	.4
$(BiYb)_3 (Fe)_5 O_{12}$	1011	12195	6527	1.87
	1010	10514	7661	1.37
	1012	6410	5356	1.12
$Bi_2O_3 - PbO$ Melt	1013	9760	6310	1.55
	1014	11702	5320	2.20
	1016	14216	6447	2.20
	1020	12500	8803	1.42
161D	6102	6447	7089	.91
	6103	5646	6209	.91
$(BiYb)_3 (FeGa)_5 O_{12}$	6107	8526	4108	2.08
	6109	9049	3701	2.44
$Bi_2O_3 - Na_2O$ Melt				
163	1048	25688	11036	2.34
$(BiYb)_3 (FeAl)_5 O_{12}$	1049	16349	8224	1.99
	1050	11375	6069	1.87
$Bi_2O_3 - Na_2O$ Melt	1052	23890	10524	2.27
	1053	16940	7222	2.34

making comparisons is by taking the average value of $\frac{F}{B}$ for each group. This is tabulated below in Table 8.

TABLE 8.

Sample Group	Type	F/B
1001-1021	Bi-Ga doped, Pb flux	.74
102-109	Bi-Ga doped, Na flux	1.58
1009-1020	Bi doped, Pb flux	1.61
1048-1054	Al doped, Na flux	2.19

The 1009-1020 and 1048-1054 groups show an average figure of merit that is somewhat larger than for garnet groups 1001-1021 and 102-109. One observation is that a sodium flux system improves the Faraday rotation more than it worsens the absorption. Further investigation needs to be done before concluding that sodium augmented melts are superior to lead melts.

D.   Magnetization and Anisotropy

The starting point for magnetic characterization of magneto optic garnet films is the determination of the magnetic moment per unit volume of the material. Knowledge of $4\pi M$ is basic to the understanding of the demagnetized or stripe domain state of iron garnet thin films because it determines how light will be deflected and how the domains will respond to applied magnetic fields.

Figure 13 is a pictorial of a typical bismuth substituted ytterbuim iron garnet thin film as seen with a polarizing microscope. If a small magnetic field is applied normal to the platelet one set of domains, say the light set, grows by wall motion with respect to the other set. As the field is increased the dark set of domains diminish in width until they appear to be simply lines as shown in Figure 14. A slight further increase in field spontaneously causes the lines to break up into segments and as the applied field
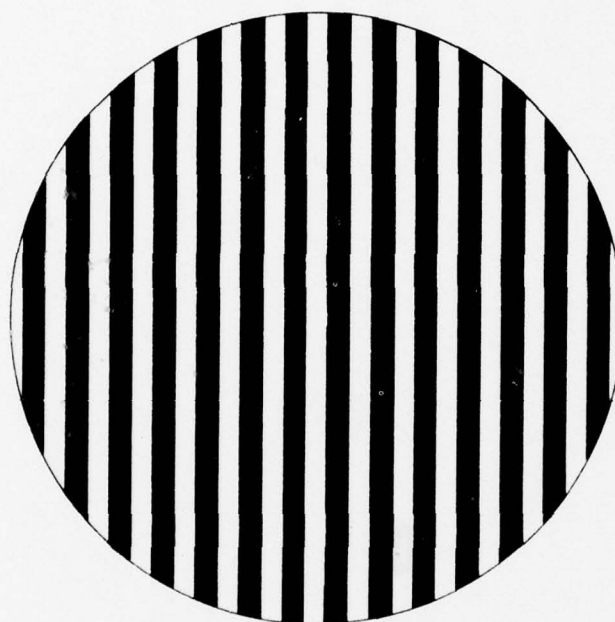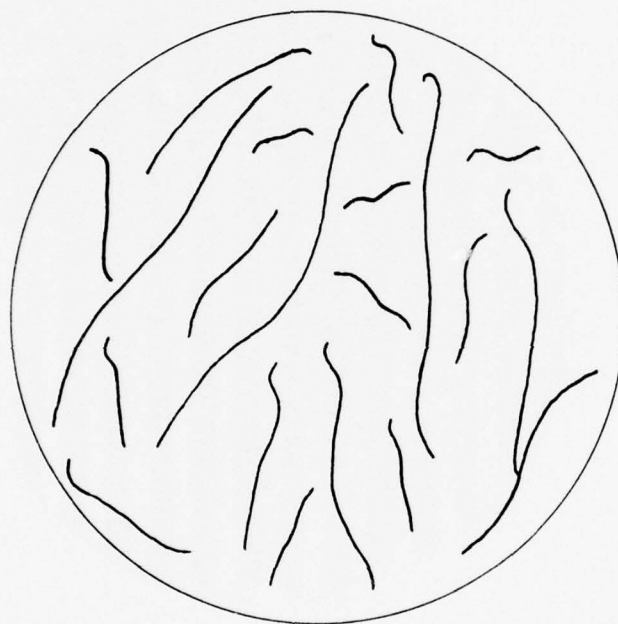
32

Figure 13. Demagnetized Stripe Domain Configuration

33

WHITE DOMAINS HAVE GROWN AT THE
EXPENSE OF THE DARK DOMAINS.

Figure 14. Domains

34

continues to increase the segments shrink to nice stable bubbles as shown in Figure 15. This process is somewhat similar to the bubble garnet materials. There is one difference, however, and that is, that the bubble garnets require an additional field to more efficiently cause the thin lines to break up into segments. It does suggest, though, that the bubble state of both stripe domain and bubble garnets can be characterized by similar theory. Since techniques have been developed for measuring the magnetization in bubble films it was reasonable to extrapolate those techniques to the determination of $4\pi M$ in stripe domain garnets. Fortunately the theory of bubble magnetization can be simplified quite a bit for stripe domain magnetization as the following analysis will show.

One parameter of special interest in bubble work is the material length, λ, defined as:

$$\lambda = \frac{\sigma}{4\pi M_s^2}$$

where σ = the wall energy density

and M_s = the saturation magnetization moment.

Magnetization curves for various values of λ with respect to film thickness have been calculated and these curves show that when λ is very much smaller than film thickness the following equation in the applied field is relevant:

$$\frac{M}{M_s} = \frac{H}{4\pi M}$$

or simply $4\pi M$ equals the applied field, H. This is a remarkable result and suggests an easy way of measuring $4\pi M$ provided that λ can be shown to be much smaller than thickness in stripe domain garnets. Starting from the equations

$$\lambda = \frac{\sigma}{4\pi M_s^2}$$

35
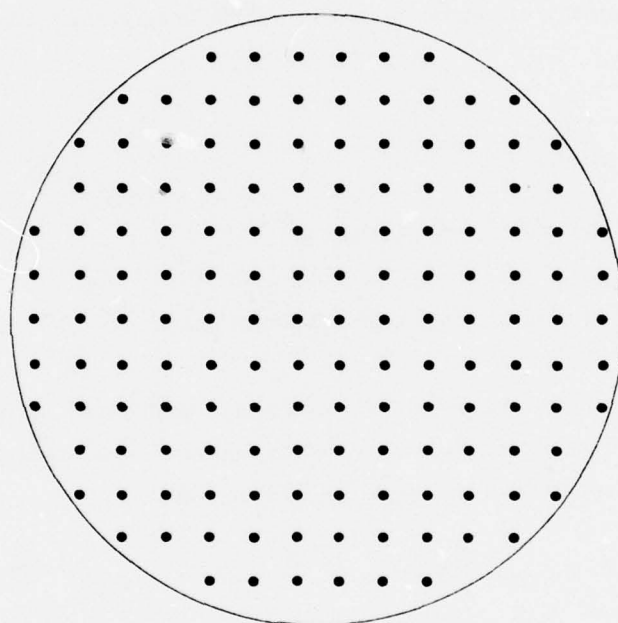
RAFT OF METASTABLE, UNIFORM, EQUIDISTANT
BUBBLES

Figure 15. Domain Raft

36

and $\qquad \sigma = (2 \, A \, H_k \, M)^{1/2}$,

and letting

$\qquad H_k = 100 \, Oe \equiv$ anisotropy field

$\qquad M = 100 \, Oe$

$\qquad A = 10^{-6} \, \dfrac{erg}{cm^3} \equiv$ exchange constant:

then for stripe domain films $\lambda \sim 10^{-2}$ microns. Typical film thickness is about 5 microns, so that λ is about 500 times smaller than thickness. This is sufficiently close to the theoretical straight line magnetization curve of reference 16 to justify taking $4\pi M$ as the normal field necessary to just saturate a film.

Because of this conclusion the apparatus of Figure 16 was constructed. The sample to be tested is placed inside the air core solenoid that is water or perhaps steam cooled. The coil consists of 275 turns of 10 gauge copper magnet wire and is capable of supporting a field of 2700 oersteds with existing power supplies. Polarized light @ 6328 Å from the helium-neon laser is passed through the sample and into the objective lens of the microscope. An analyzer inside the microscope is set at 45° to the polarizer and the Faraday rotated light is then sensed by the photodiode/eyepiece combination. A sample of the incident beam is used as a normalizing coefficient to keep the laser output variations from masking the true signal. The output of the normalizing circuit is placed on the ordinate of a Hewlett Packard model 135 X Y plotter. Abscissa data is taken from a sample of the coil current. The measurement is done by first slowly increasing the coil current in one polarity until magnetic saturation of the film is achieved as indicated by the vanishing of the first variation of Faraday rotation with respect to applied field. Next the current is retraced to zero and any deviation of the curve as the film comes out of saturation is an indication of magnetic hysteresis. Finally the polarity of the applied field is reversed and the experiment rerun to trace out the other half of the loop. The value of $4\pi M$ is, then, readily obtainable from the loop and, in addition, a permanent record of the magnetic features of the film has been gotten. Figure 17, a curve run for an in-house grown stripe sample, does yield a value for $4\pi M$ that can be accepted with confidence.
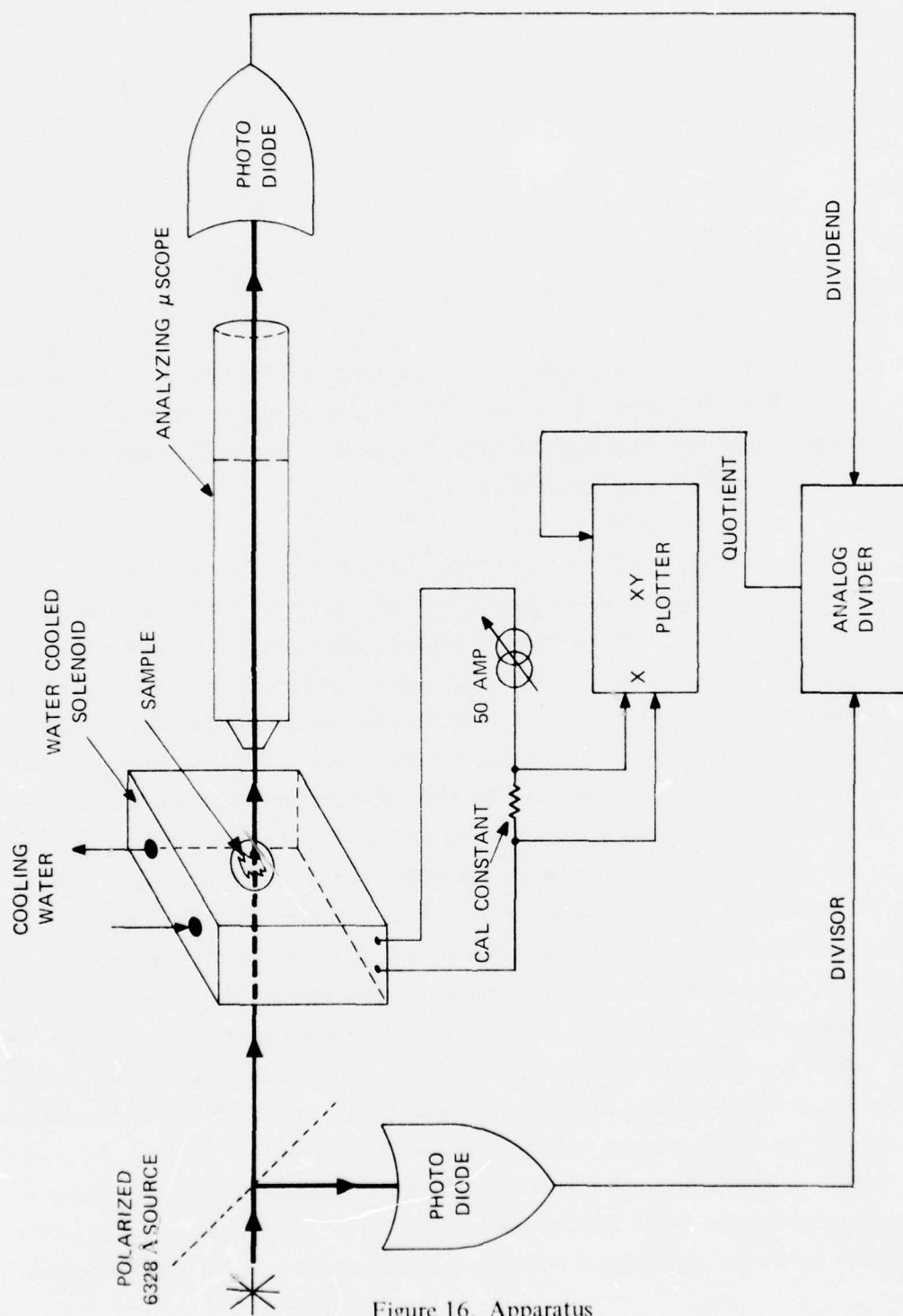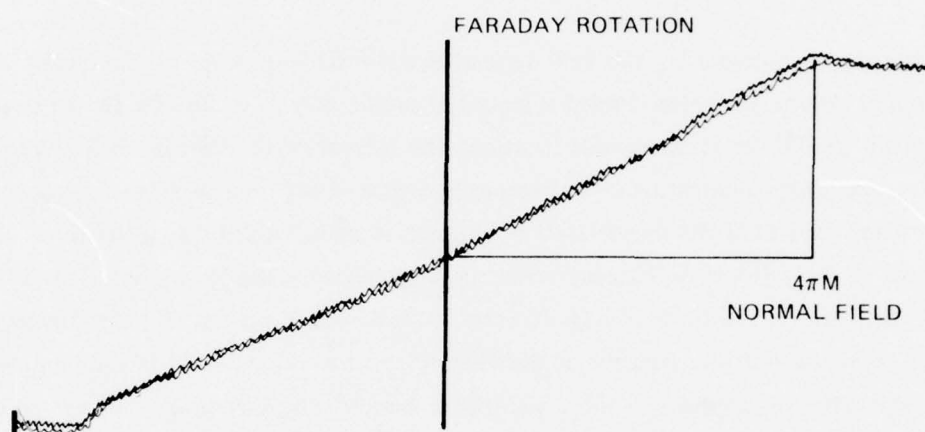
Figure 16. Apparatus

38

Figure 17. Faraday Rotation vs. Normal Field Used to Measure $4\pi M = 1403$ Oe for Crystal 1012

Knowledge of numerical values of the anisotropy field H_k is important because the deflector drive field is proportional to H_k. Furthermore, knowledge of numerical values for the anisotropy field, H_k, in stripe domain films is important because of all the equations that require this parameter as a coefficient. This includes the wall width, all energy, wall response to an applied field, anisotropy constants, and probably other quantities that may become apparent as stripe domain theory evolves. The simplest method of ascertaining the value of H_k is to determine the strength of an in-plane field that is just sufficient to draw the magnetization into the plane of the film. Although the response of the magnetization to an in-plane field is highly nonlinear, the endpoint nevertheless describes the magnitude of H_k.

In order to measure H_k the $4\pi M$ apparatus was modified. A set of Helmholtz coils was wound around the water cooled solenoid in such a way as to provide for an in plane field of up to 300 Oe at the sample location. The measurement is made setting the polarizer analyzer combination to extinction and then slowly increasing the current to the in-plane coils until the magnetization is drawn in plane. Again this is indicated by the vanishing of the differential Faraday effect as pinpointed by the photodiode sensor. The field is then slowly returned to 0 Oe to identify hysteretic processes. Finally, the experiment is repeated with the polarity of the field reversed in order to aid in the elimination or understanding of anomalies in the apparatus or sample. Since the data is displayed on an X Y plotter, a permanent record of the films response to an in-plane field is obtained. Figure 18 is such a document and it was gotten from one of the in-house fabricated stripe domain garnet films.

In comparing Figure 18 and Figure 17, a stripe sample magnetizations curve, it is reasonable to question the much larger apparent hysteresis in the H_k measurement. Because the scale factor on the abscissa of the H_k graph is five times as sensitive as that of the $4\pi M$ graph, the H_k graph can yield much greater detail. It is safe to assume that the actual hysteresis in both the H_k loops and the $4\pi M$ loops are approximately equal for any sample.

Table 9 gives $4\pi M$ and H_k values for (bi Yb) Fe garnet films from melt 151, a Bi_2O_3PbO melt, and values for $(BiYb)_3 (FeAl)_5$ garnet films from melt 163, a $Bi_2O_3 - Na_2O$ melt. In Table 9, a blank indicates Hk data was not obtained.
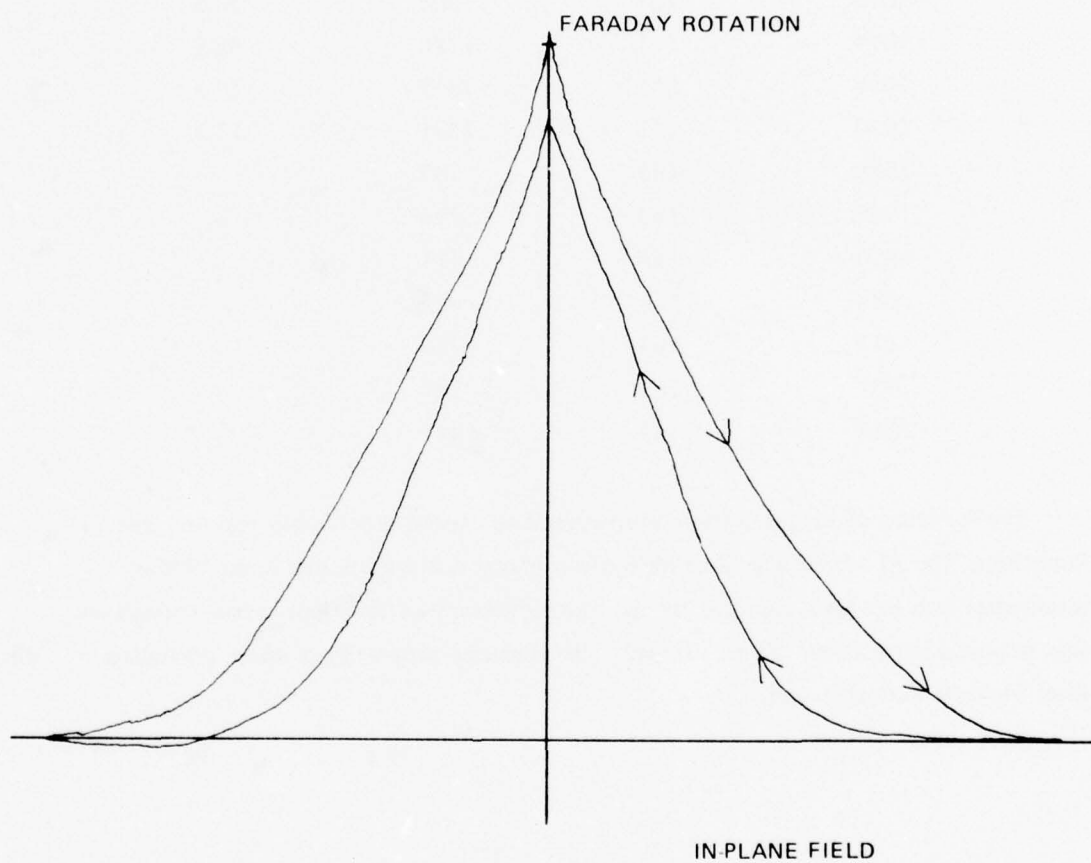
40

Figure 18. Faraday Rotation vs. In Plane Field Used to Determine H_k = 151.3 Oe for Crystal 1020

41

TABLE 9. MAGNETIZATION AND ANISOTROPY

Crystal	Melt	$4\pi M$	H_k
1009	151	1675	–
1010	151	1361	–
1011	151	1486	49.6
1012	151	1403	–
1013	151	1508	92.5
1014	151	1780	98.2
1016	151	1675	27.5
1020	151	1591	15.3
1048	163	737	–
1049	163	714	–
1050	163	811	–
1052	163	921	–
1053	163	770	–
1051	163	767	–
1054	163	419	–

The variation of magnetization from crystal to crystal is probably real and due to impurities. The Al containing films have lower magnetization because some of the tetrahedral iron has been replaced by Al. The anisotropy of the films is low enough so that practical drive fields can be utilized. The magnetic properties of these crystals is ideal for light deflector uses.

SECTION IV
GRATING CHARACTERIZATION – BEAM DIVERGENCE

Beam Divergence

The first order diffracted beam is a collection of smaller discrete beams.[1,2] The individual sub-beams have an angular divergence ~ 1 mr and the total collection has a divergence of ~ 10 mr. In addition, the following effects have been observed:

a) The zero order beam is not noisy which implies the substrate is uniform and the film has uniform thickness with respect to index, pathlength, etc.

b) If the crystal is translated past an aperture the light intensity in the sub-beams changes. So, there exist discrete regions of non-uniform grating.

c) A change of applied magnetic field causes some sub-beams to move more than others. This can be explained by independent switching of separate regions.

What can be done to analyze the diffraction? The diffraction equation is.

$$\sin \theta = \frac{n\lambda}{2d}$$

Differentiation yields

$$\cos \theta \; \delta\theta = \frac{-\lambda}{2d^2} \; \delta d$$

or $$\delta d = -2 \frac{\cos \theta \; d^2}{\lambda} \; \delta\theta$$

for $\lambda = 6328 \text{ Å}$
$\theta = 20° = .35 \text{ rad}$
$d = 0.93 \; \mu m$

and $\delta d = 2.5 \; \delta\theta \; \mu m$ (1)

43

If $\quad \delta\theta = 10^{-2}$ rad = 10 mr,

then $\quad \delta d = .025 \ \mu m$ $\qquad\qquad\qquad\qquad\qquad\qquad\qquad\qquad$ (2)

If $\quad \delta\theta = 10^{-3}$ rad = 1 mr,

then $\quad \delta d = .0025 \ \mu m$ $\qquad\qquad\qquad\qquad\qquad\qquad\qquad\quad$ (3)

Thus we cannot simply look at domains with a microscope because with visible light we will not see features of this scale in any one domain.

What we can do is to note that for $\delta\theta = 10$ mr, $\delta d = 2.5\%$, or 1 part in 40. We can then look for something in the crystal that would cause such a small variation. We set out to find defects with a density of one every 40 domains. What we discovered was an unusual magnetic configuration: a domain vertex, Figure 19. In a demagnetized state, the vertex domain could always be associated with a film defect, although the defect may be remotely located. The vertices move when the field changes. The domains bend near the vertex. However, far from the vertex they are unperturbed. So, there is one more of each domain in the grating region in the left side of Figure 19 than in the right side of Figure 19. The grating on the left side contains one additional period. If there are N+2 stripes on the left side, then there are only N stripes on the right side. As a result the diffraction angle is ~10 mr larger on the left. Experimentally it was observed that frequently $N \gtrsim 40$.

When a magnetic drive field increases, the vertex moves to increase the area which has one more domain and reduce the area which has one less domain. In Figure 19 the vertex moves to the right as the applied magnetic field increases. This motion is one way the number of domains in the film increases. For the purpose of a high resolution deflector, it is imperative that the aperture in the crystal contain no vertices. Thus if the film is to be allowed to switch by vertex propagation, the vertex ought to be kept out of the aperture, if possible, or ought to be caused to move as rapidly as possible across the aperture.
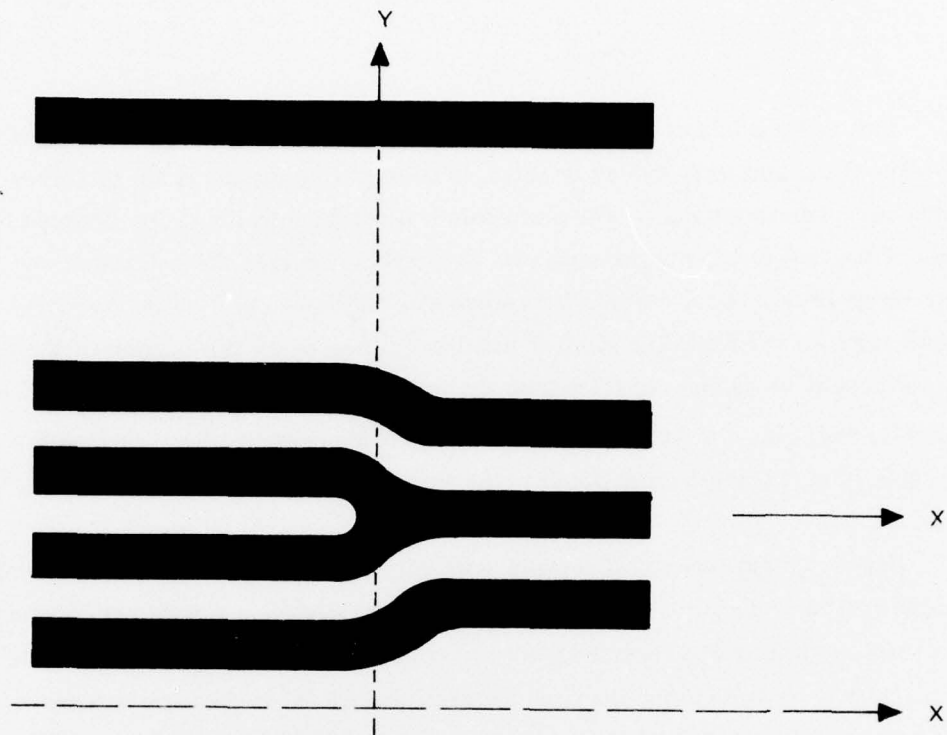
44

FIGURE 19 VERTEX: ONE MORE WHITE AND ONE MORE BLACK DOMAIN EXIST IN THE LEFT SIDE THAN IN THE RIGHT SIDE. FAR FROM THE VERTEX IN THE Y-DIRECTION, THE DOMAINS ARE STRAIGHT. SO, THE GRATING CONSTANT ON THE LEFT SIDE IS A FEW PERCENT HIGHER THAN ON THE RIGHT SIDE, AND THE DIFFRACTION ANGLE FOR LIGHT PASSING THROUGH THE LEFT SIDE IS ~10 MR LARGER THAN THE ANGLE FOR THE RIGHT SIDE.

Figure 19. Vertex Domains

45

Two vertex domains can oppose each other as in Figure 20. When this happens a portion of the grating is rotated or tilted, but the grating spacing is not perturbed as when only one vertex exists. The perturbation is confined to the region between the two tips. If the two vertex tips are separated by N~50 domains in the y-direction and if both tips lie on or near the x = 0 line, the grating will be tilted away from the x-axis by small angle $\delta\phi \sim 10$ mr. The result is that light diffracted by this portion of the grating is not parallel to the light diffracted by the rest of the grating. The angle or deviation is $\delta\psi = \sin\theta\,\delta\phi$; here, θ is the polar diffraction angle, see Figure 21. Since $\sin\theta \sim .5$, $\delta\psi \cong 5\text{-}10$ m rad, which corresponds to the angular azimuthal separation observed.

Experimentally one way that many vertex domains can be created is by applying a magnetic field to the stripe domains which have been lined up in a different direction by the prior application of a magnetic field. Sometimes the domain structure will rotate coherently in response to the field, see Figure 22 and 23. When the angle between the directions of first and second field direction is more than about $45°$, then the stripes buckle rather than rotate coherently, see Figure 23. This results in the formulation of numerous vertices, see Figure 24. By increasing the field magnitude in the new direction, or by applying a hysteresis field, most of the vertex domains are removed. The ones that do not erase are attached to crystal defects, e.g., scratches, inclusions, pits, or edges.

Photomicrographs of vertex domains are presented. The first set show individual vertex domains; the second set show the resultant dark field grating image. Figure 25 shows two vertices. The influence of the vertex extends along the line A—A^1 for about 80 domains, and along B–B^1 for about 82 domains. The distance between the points A1 and A2 equals the distance between B1 and B2. The domains are ~3 μm wide. The second vertex in Figure 25 shows a similar grating perturbation.

Figure 26 shows how the domains respond to a small ~10 Oe field. One vertex has moved out of the field of view. The other has moved and is being overtaken by a second vertex. A third vertex is visible in the corner. It is moving in from the opposite direction.
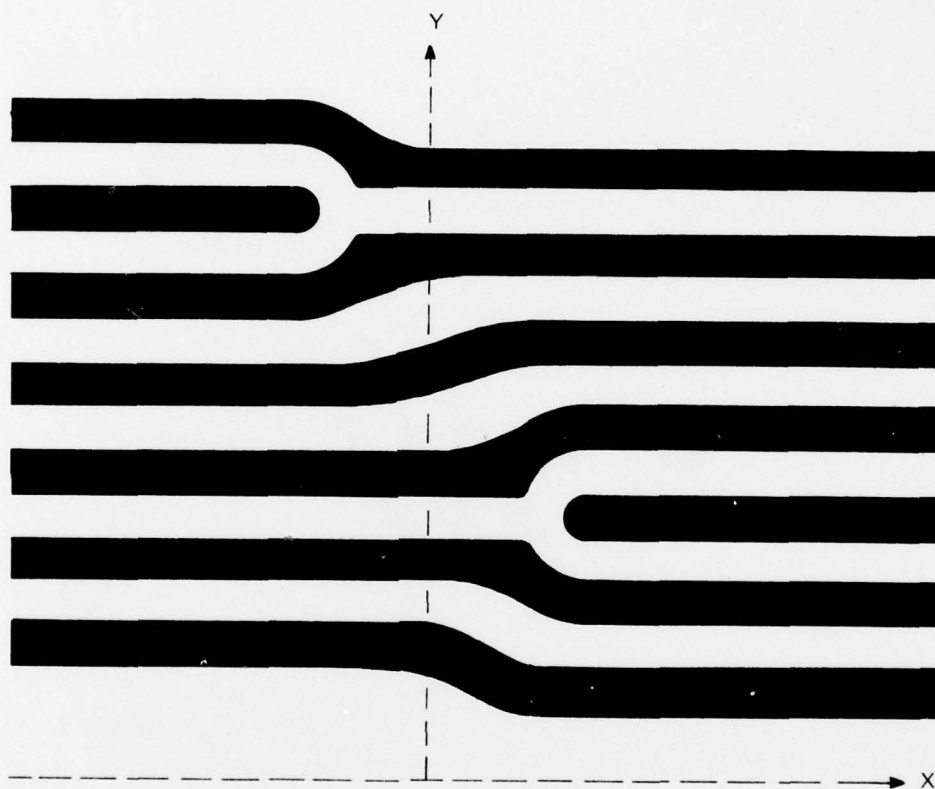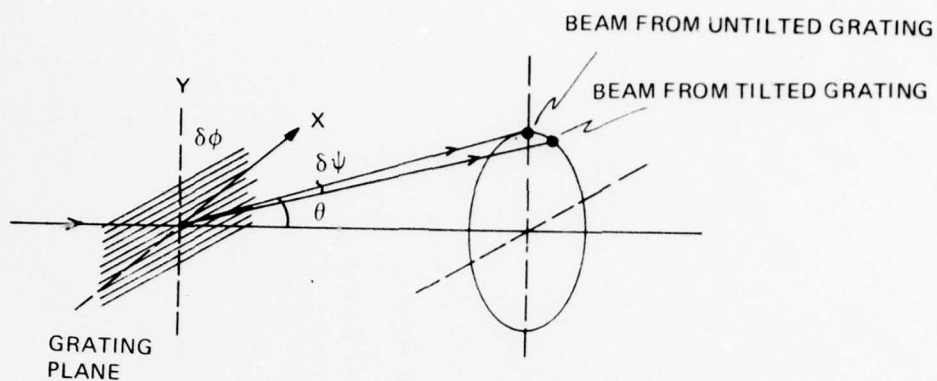
46

Figure 20. Vertex Pair

47

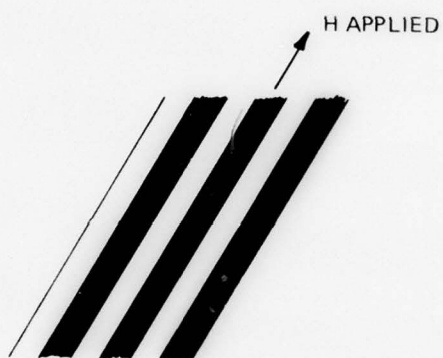Figure 21. Angular Divergence

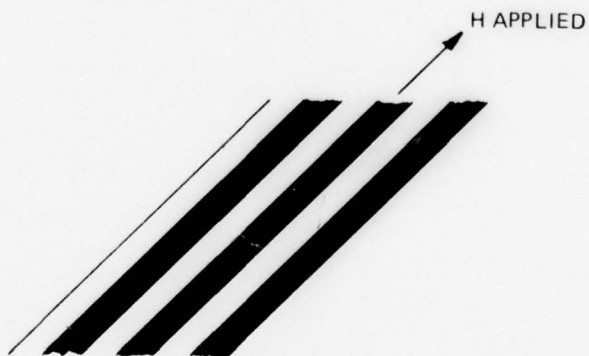Figure 22. Uniform Domains

Figure 23. Coherent Domain Rotation

48

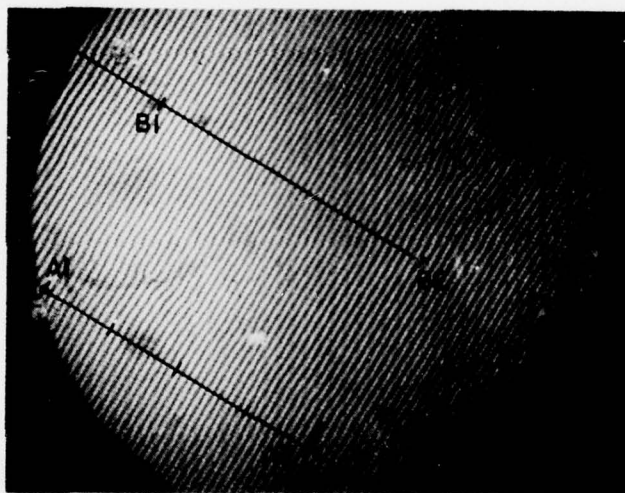Figure 24. Vertex Formation
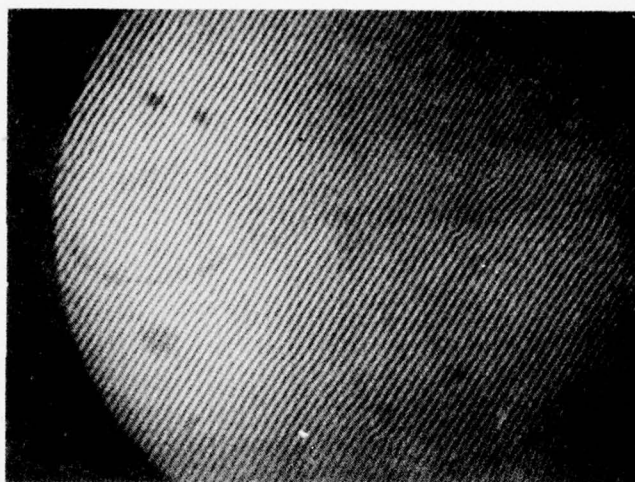

Figure 25. Vertex Domains

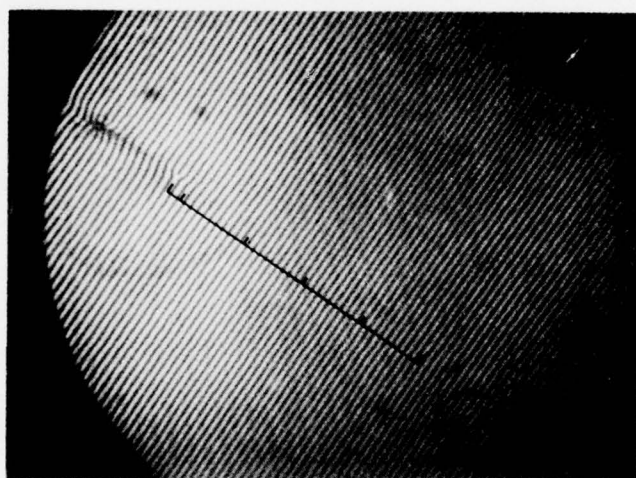Figure 26. Vertex response to field change

Figure 27. Vertex near defect

50

Figure 27 shows a single vertex near a large film defect. The influence of this vertex extends about 80 domains in the direction away from the defect. A small point defect can be seen in the encircled region. The domains are bent in the immediate vicinity of this defect.

Figure 28 shows the creation of numerous vertices by buckling. The domains were initially lined up from 1 o'clock to 7 o'clock. The buckling results from the application of a field 55° clockwise from the initial direction. The previous figures, 25,26,28,27, are photos of the same region of the source film. It is evident that all but a few vertices were removed (the photo in Figure 28 was taken before 25,26,28, and 27 were taken).
Figure 29 shows several stages of vertex formation. This pattern is generated by applying a 60 Hz alternating field obliquely to the crystal plane. As before, all but a few are erasable.

The next set of figures show an image of the grating in a crystal viewed with a microscope and crossed polarizers. The light in the image is all contained in the first order diffraction spots. The analyzer blocks the central spot and the objective lens aperture blocks the higher order diffracted spots. So the image is created entirely by first order diffracted light. Figure 30 shows an image of a portion of the crystal with zero applied field. It is bright except for a dark scratch. Figure 31 shows the same crystal region with a small in-plane magnetic field. Dark bands are visible. At the leading edge of each dark band is a vertex. Many domains are contained in each band; the bands are parallel to the domains. The bands are dark because the objective aperture discriminates against the large diffraction angle of the light from the band. As the field is increased, the bands advance across the crystal. Figure 32 shows the same region with a larger field. Both this figure and the last clearly show the discrete nature of the grating. Finally Figure 33 shows the region with a large field. It is uniformly dark.

Thus, in conclusion, a reason for the structure in the first order beam has been identified. The existence and motion of vertex domains accounts for most of the structure. The vertex domains can be erased by applying a large field, except whenever they are tied to film defects. It is clear that the optimum grating contains no vertex in the aperture area. So, if the grating period is to be changed by vertex motion either 1) the vertexes must be confined to a region outside of the aperture or 2) the vertex velocity must be very large. It is our judgement that the vertex domains can be controlled in one of these two ways.
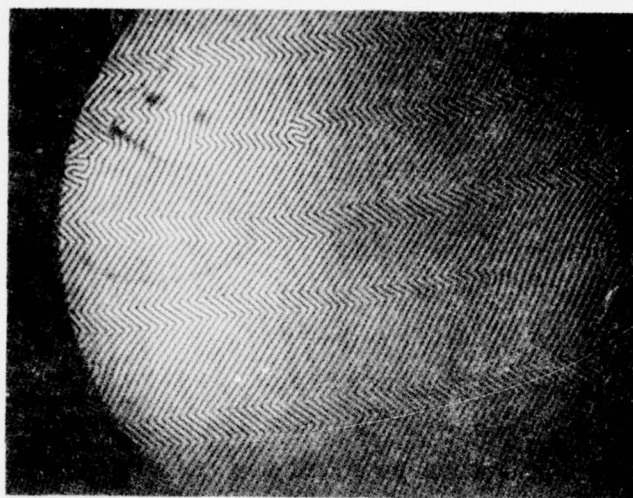
51

Figure 28. Buckling of domains
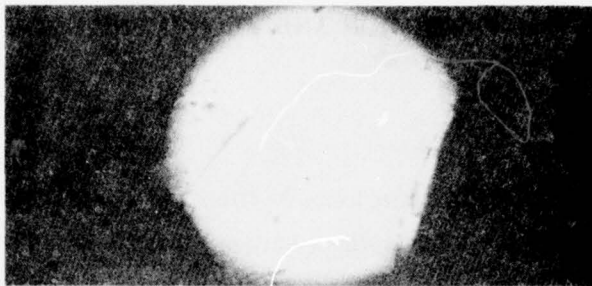

Figure 29. Vertex formation

52
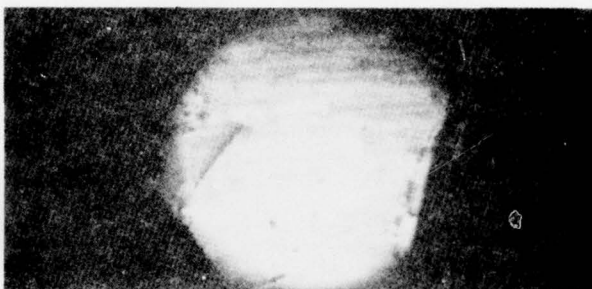
Figure 30. Zero field grating image

Figure 31. Dark bands in grating image

Figure 32. Dark bands in grating image

Figure 33. Saturated grating

53

SECTION V
CONCLUSION AND RECOMMENDATION

A.   Conclusions

Strain-free, crack-free epitaxial bismuth ytterbium garnet deflector crystals can be grown on GGG substrates in melts which contain either Na_2O or PbO in addition to Bi_2O_3. The state of strain in the epitaxial crystal depends not only on growth temperature but also on melt composition. The addition of Na_2O or PbO to the melt is required not only to reduce the growth temperature but to facilitate growth of the epitaxial crystal subject to a large compressive strain by the substrate. The compressive strain which exists during growth offsets the tensile strain imparted by differential thermal expansion rates during cool-down to room temperature. In this way strain-free, crack-free deflector crystals are obtained.

The cause of beam divergence which limits the number of resolvable spots in the crystals grown for this contract has been identified. The grating periodicity is perturbed by a vertex domain structure. The vertex domains separate the grating into regions; each region has a slightly different grating constant and orientation. Control of the vertex domains should be eminently possible by tailoring the edges of defect-free crystals. In other respects the magnetic properties of the deflector crystals are ideal for stripe domain grating formation.

The Farday rotation of the crack-free crystals is as large as expected; the largest measured 6328 Å specific rotation was over 25,000 deg./cm. The large rotation is necessary for an efficient deflector. Faraday rotation in excess of 3000 deg/cm was measured for two crystals at 1.06 μm. The 1.06 μm optical absorption of a few of the crystals is less than 100 db/cm. The absorption mechanism is not understood but is probably due to electronic transitions among impurity, band-gap states. Obtaining crystals with 100 db/cm or less absorption consistently will be, in our judgement, a far simpler task than was obtaining crack-free crystals.

54

B.   Recommendations

The difficult crystal problem (cracking) has been solved. Accordingly, we recommend that the next steps be taken. Specifically, at the same level of effort a 10^6 spot, 50% efficient 1.06 μm laboratory deflector can be achieved by:

1.   Diminishing beam divergence by vertex domain control

and

2.   Diminishing optical losses to less than 100 db/cm absorption.

Based on the past effort, these tasks are tractable.

We believe that a 10^8 spot, 80% efficient deflector will necessarily follow from such an effort.

REFERENCES

[1] Technical Report AFAL-TR-72-396 (March 1973)

[2] Technical Report AFAL-TR-74-183 (September 1974)

[3] Technical Report AFAL-TR-75-122 (August 1975)

[4] H. Takevelir et al, J. Appl. Phys., 44, 4789, (1973)

[5] D. Lacklison, et al, I.E.E.E. Trans., Magn. MAG-9, 45F, (1973)

[6] J. Dillon, Jr. et al, J. Phys. Chem. Solids, 27, 1531 (1966)

[7] F. S. Chen, et al, Phys. Rev. Lett., 19, 948 (1967)

[8] A. Akselrad, R. E. Novak, D. L. Paterson, A.I.P. Conf. Proc., 18, 949-953, (1973)

[9] S. Witterock, J. M. Robertson, T. J. A. Popma, P. F. Bongers, A.I.P. Conf. Proc., 10, 1418 (1972)

[10] P. Besser, et al, A.I.P. Conf. Proc., 5, 125-9 (1971)

[11] P. Besser, et al, Mat. Res. Bull., 6, 1111, (1971)

[12] H. Makino, et al, A.I.P. Conf. Proc., 18, 80, (1973)

[13] S. Geller, et al, Mat. Res. Bull., 7, 1219 (1972)

[14] Shanon and Pruitt

[15] Levin and McMurdie, Phase Diaglogues for Ceramists, Am. Cer. Soc., 1964 Fig. 323.

[16] Bobeck, De La Torre